

ELEKTROTEHNIČKI FAKULTET  
UNIVERZITETA U BANJALUCI

---

*FACULTY OF ELECTRICAL ENGINEERING  
UNIVERSITY OF BANJALUKA*

# ELEKTRONIKA

# *ELECTRONICS*

YU ISSN 1450-5843

GODIŠTE 7, BROJ 1, SEPTEMBAR 2003. *VOLUME 7, NUMBER 1, SEPTEMBER 2003.*

# FACULTY OF ELECTRICAL ENGINEERING UNIVERSITY OF BANJALUKA

Address: Patre 5, 78000 Banjaluka, Republic of Srpska, Bosnia and Herzegovina

Phone: + 387 51 211-408, + 387 51 221-820

Fax: + 387 51 211-408

## ELECTRONICS

e-mail: elektronika@etfbl.net

*Editor:* Prof. Branko L. Dokić, Ph. D.  
Faculty of Electrical Engineering  
University of Banjaluka, Republic of Srpska  
e-mail: bdokic@etfbl.net

### *Program Committee:*

- Nikolaos Uzunoglu, National Technical University of Athens, Greece
- Barry Jefferies, University of Hertfordshire, UK
- Vojin Oklobd`ija, University of California, Davis, USA
- Bratislav Milovanovi}, Faculty of Electronics Niš, FR Yugoslavia
- Mili} Stoji}, Faculty of Electrical Engineering Beograd, FR Yugoslavia
- Vojislav Aran|elovi}, Institute "Vinča" Beograd, FR Yugoslavia
- Veljko Milutinovi}, Faculty of Electrical Engineering Beograd, FR Yugoslavia
- Ilija Stojanovi}, SANU Beograd, FR Yugoslavia
- Vladimir Kati}, Faculty of Technical Sciences Novi Sad, FR Yugoslavia
- Aleksandar Ili{kovi}, Faculty of Electrical Engineering Banjaluka, RS
- Milorad Bo`i}, Faculty of Electrical Engineering Banjaluka, RS

*Secretary:* Petar Matić, M.Sc.  
e-mail: pero@etfbl.net,  
Faculty of Electrical Engineering  
University of Banjaluka, Republic of Srpska

*Publisher:* Faculty of Electrical Engineering  
University of Banjaluka, Republic of Srpska  
Address: Patre 5, 78000 Banjaluka, Republic of Srpska, Bosnia and Herzegovina  
Phone: + 387 51 211-408, + 387 51 221-820  
Fax: + 387 51 211-408  
<http://www.etfbl.net>

Number of printed copies: 150

## PREFACE

Symposium INFOTEH<sup>®</sup>-JAHORINA is continuation of the International symposium JAHORINA that was held last time on April 1991.

The main organizer of the Symposium is the Faculty of Electrical Engineering Srpsko Sarajevo and the co-organizer is the Faculty of Electrical Engineering Banja Luka. The Symposium is supported by The Faculty of electrical engineering, Beograd, the Faculty of electronics, Niš, the Faculty of technical sciences, Kosovska Mitrovica, the Faculty of electrical engineering, Podgorica, the Faculty of technical sciences, Novi Sad.

The goal of the Symposium is the multidisciplinary survey of the actual state in the information technologies and their application in the industry plants control systems, the communication systems, the manufacturing technologies, power system, as well as in the other branches of interest for the successful development of our living environment.

During the first Symposium INFOTEH<sup>®</sup>-JAHORINA 2001, that was held on 12-14 March 2001 in the hotel Bistrica at Jahorina, 53 works have been presented, six companies presented their development and manufacturing programs in telecommunications, power electronics, power systems and process control systems. More than hundred participants took part in the Symposium working. Round table about potentials and possibilities of economic cooperation between Republic of Srpska and FR Yugoslavia has been held during the Symposium, regarding successful appearance at domestic and foreign market.

During the second Symposium INFOTEH<sup>®</sup>-JAHORINA 2002, that was held on 25-27 March 2002, 76 works have been presented, and five companies presented their development and manufacturing programs. More than hundred and thirty participants took part in Symposium working. Round table entitled "Reforms in high education – step forward to the European University" has been held during the Symposium.

The third Symposium INFOTEH<sup>®</sup>-JAHORINA 2003 was held on 24-26 March 2003 in the hotel Bistrica at Jahorina. The main topics of the Symposium were: Computer science application in control systems, Information-communication systems and technologies, Information systems in manufacturing technologies, Information technologies in power systems, Information technologies in other branches of interest. More than hundred and fifty participants took part in the Symposium working, coming from Serbia, Montenegro, United Kingdom and Republic of Srpska. At the Symposium 73 papers have been presented and nine student papers. Four companies presented their development and manufacturing programs. Round table entitled "New Technologies and Industrial Production Capabilities for small Countries in the Transition Process" has been held during the Symposium. Prof. Dr Miloško Lazić, IRITEL Telecommunications and Electronics Co. Beograd gave the introductory talk and invited paper. All papers are presented in symposium proceedings, CD version.

This issue of international journal "Electronics" includes ten the most interesting papers selected from the third Symposium INFOTEH<sup>®</sup>-JAHORINA 2003.

I would like to invite all readers of the "Electronics" journal to take active participation at the next Symposium INFOTEH<sup>®</sup>-JAHORINA. Updated information can be obtained from the Symposium web page: <http://www.infoteh.rs.ba>.

Prof. Dr Slobodan Milošković

Chair, INFOTEH<sup>®</sup>-JAHORINA 2003 Programme Committee

INFOTEH<sup>®</sup>-JAHORINA 2003 Organization Committee

## BIOGRAPHY OF PROF. DR SLOBODAN MILOJKOVIĆ



Slobodan M. Milojković was born in Belgrade, Serbia and Montenegro on 26 June 1941. He received the B.Sc. and M.S.E.E. degrees from the University of Belgrade in 1963, 1975, respectively, and Ph.D. degree from the University of Sarajevo in 1978. In January 1964, he joined the Institute of Thermo Technique and Nuclear Technique, Energoinvest, Sarajevo, where he worked in modeling and numerical simulation in the various physical processes: nuclear technique, thermo technique, electrical engineering, electrochemistry, electrothermal engineering, electromagnetic. In September 1964, he began academic career as an honorary lecturer in the Faculty of Electrical Engineering. In May 1970, he was an honorary docent, teaching courses in theoretical electrical engineering. In January 1981, he joined the Faculty of Electrical Engineering, University of Sarajevo, where he is presently Full Professor, teaching courses in theoretical electrical engineering. From October 1994 to April 1996, he worked as a Guest Professor at Technical University of Munich in High Voltage Institute. During that time, he was working on the development of the software modules for modeling, calculation and visualization of electromagnetic fields in high voltage equipment. The Asea Brown Boveri AG Research Center, Heidelberg, used those newly created modules in a software package POLOPT<sup>®</sup>. He led research projects supported by international organizations and commercial enterprises. His current research interest involves the computer-aided design of electromagnetic devices. Dr S. Milojković is one of the authors of monograph "Integral Methods for the Calculation of Electric Fields, for Application in High Voltage Engineering", Scientific Series of the International Bureau Research Center Juelich - Germany, 1992, ISBN 3-89336-084-0. He is also author of 6 books and over 10 scientific journal papers, 30 conference papers and 70 research projects. He was the supervisor of nearly 70 Diploma engineering thesis, 15 Master thesis and 4 Ph.D. thesis. Dr S. Milojković was awarded the Prize of the enterprise Energoinvest Sarajevo, the Gold medal of Technical Military Academy Rajlovac, the Gold diploma of the Faculty of electrical engineering Sarajevo, the Diploma of the Faculty of electrical engineering Tuzla, the Gold diploma of the University Sarajevo.

## OPTICAL FLIP-FLOP OSCILLATOR WITH COMPLEX COUPLING CONSTANT

Zoran Ljuboje, Faculty of Electrical Engineering Srpsko Sarajevo  
Milan Petrović, Institute of physics Zemun

**Abstract:** Model of optical flip-flop oscillator, realized by two coupled photorefractive oscillators, has been analysed. The coupling strength in this geometry is a complex number, because of the presense of external electric field.

**Keywords:** Photorefractive oscillators, four-wave mixing, flip-flop, complex coupling strength.

### 1. INTRODUCTION

The photorefractive effect is an interesting phenomenon, caused by the interaction of laser light with some ferroelectric crystals, and this part of physics is called photorefractive optics. Basic equations which describe the processes in photorefractive crystals are given by Kukhtarev, Markov and Odulov, 26 years ago [1]. Photorefractive effect includes the light-induced periodic changes of refractive indices in electro-optic crystals when diffraction grating is formed. One of the basic processes in the crystal is the four-wave mixing (FWM) of laser beams, shown in Fig.1.

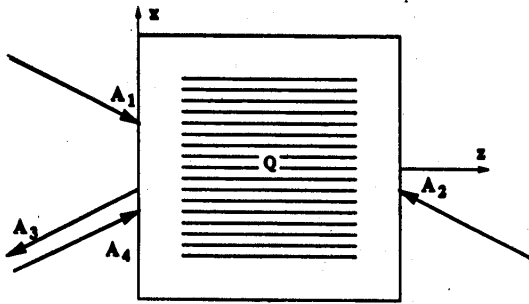


Fig.1: FWM in photorefractive crystals.

### 2. DESCRIPTION OF THE PROCESS

In this process crystal is illuminated with three laser beams: two parallelly polarized and oppositely directed pumps with amplitudes  $A_1$  and  $A_2$ , and incident signal  $A_4$ . Nonlinear interaction of these fields leads in this manner to the building of diffraction gratings in the interaction region of the crystal. As a result, the fourth wave with amplitude  $A_3$  is established, which represents the phase conjugate replica of beam  $A_4$ . In other words, beam  $A_3$  is the reflected incident beam  $A_4$ , but returned the same way as the incident beam, in distinction to the usual mirror, where the well known laws of geometrical optics apply to the reflected beam. This phenomenon is interesting because of its great potential applications.

The process of FWM is described by the equations [1]:

$$IA_1' = -\gamma QA_4, \quad IA_4' = \gamma^* Q^* A_1 \quad (1a)$$

$$IA_2' = -\gamma^* Q^* A_3, \quad IA_3' = \gamma QA_2 \quad (1b)$$

where  $A_1, A_2, A_3, A_4$  are the wave amplitudes,  $I$  is the total intensity ( $I = I_1 + I_2 + I_3 + I_4$ ), the quantity  $Q$  is the grating amplitude, and  $\gamma$  is the wave coupling constant. The prime denotes the derivative in the propagation direction  $z$ , and the asterisk stands for complex conjugation. The equation for the temporal development of  $Q$  is of the form:

$$\tau \frac{dQ}{dt} + \epsilon Q = (\gamma/I)(A_1 A_4^* + A_2^* A_3) \quad (2)$$

where  $\tau$  is the relaxation time of the grating, and  $\epsilon$  is the parameter which depends on various electric fields:  $\epsilon = (1 + E_q/E)/(1 + E_M/E)$ . The coupling constant  $\gamma$  is given by:  $\gamma = \Gamma(1 + E_q/E_D)/(1 + E_M/E)$ , where  $\Gamma$  is the driving parameter and  $E_q, E_D, E_M$  are characteristic fields which describe the crystal according to the Kukhtarev's theory [1].  $E$  is the total electric field in the crystal  $E = E_D + iE_0$ , where  $E_0$  is the external electric field applied to the crystal. If the external electric field is present, it changes the coupling parameter into complex number.

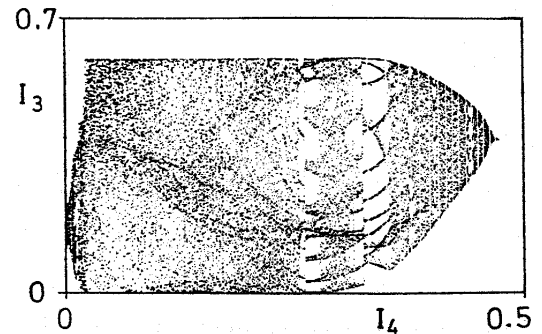


Fig.2: Reflected beam of intensity  $I_3$  as a function of the input beam intensity  $I_4$ , for the complex coupling parameter  $\gamma$ .

Practically realized devices which work on the FWM process are different photorefractive oscillators [2]. The system of equations for the operation of oscillators (1) and (2) must be investigated numerically, because they can not be solved analytically, and should be viewed with caution because of the instabilities in the solutions [3]. The case when the coupling parameter  $\gamma$  becomes a complex number affects the unstable behavior of the system. One example of such solution is given in Fig.2.

### 3. DESCRIPTION OF THE DEVICE

For the practical realization of photorefractive oscillators it is necessary to achieve stable functioning of the device. We analyze working modes of optical flip-flop oscillator in the case of complex coupling parameter.

Optical flip-flop oscillator based on FWM is realized with two interconnected ring resonators, Fig.3. One of the rings is denoted by G (for gain) and the other is denoted by L (for loss). The behavior of such a system is analogous to the behavior of electronic flip-flop, and it also represents an elementary memory and processing unit [4].

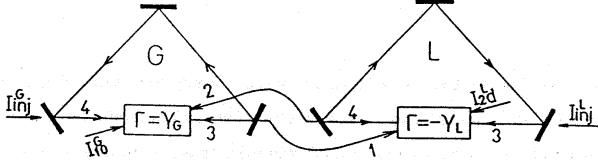


Fig.3: Photorefractive FWM flip-flop oscillator. Two photorefractive rings are competitively coupled, so that oscillation in one ring prevents the other from oscillating.

Two pumps  $I_{10}^G$  and  $I_{2d}^L$  needed to pump the crystals in a FWM scheme, are supplied externally. The rings are interconnected in such a way that a part of the intracavity energy in one ring is used to drive wave mixing in the other:

$$I_{10}^L = \alpha I_{4d}^G, \quad I_{2d}^G = \alpha I_{30}^L, \quad (3)$$

where  $\alpha$  is the fraction of energy being diverted to the other ring. The intensities of the oscillating fields in the steady state are determined from:

$$I_{4d}^G = \frac{I_{10}^G}{1 - R(1 - \alpha)} \left[ 1 - \frac{\exp(-2\gamma_G d)}{R(1 - \alpha)} \right] \quad (4)$$

$$I_{30}^L = \frac{I_{2d}^L}{1 - R(1 - \alpha)} \left[ 1 - \frac{\exp(-2\gamma_L d)}{R(1 - \alpha)} \right] \quad (5)$$

The system is so configured that oscillation in one resonator supports the pump that suppresses oscillation in the other, which is the main characteristic of flip-flop functioning. In the previous expressions R is the total reflectivity for each of the two identical resonators,  $\gamma_G$  and  $\gamma_L$  are the coupling strengths of the two crystals, and  $d$  is the width of the interaction regions in crystals.

We have analyzed the behavior of oscillator in the absence of external electric field  $E_0$ . In this case all parameters (including the coupling constants) are real numbers, and the system shows stable behavior. A typical example, for the intensity of mode  $I_{30}^L$ , is shown in Fig.4. Injecting the pulse of lower intensity requires longer times for the establishment of oscillation (and longer turn-off times for the other ring). For a given duration of the pulse, below a certain

intensity value, it is not possible to obtain oscillation. This means that a trigger threshold exists.

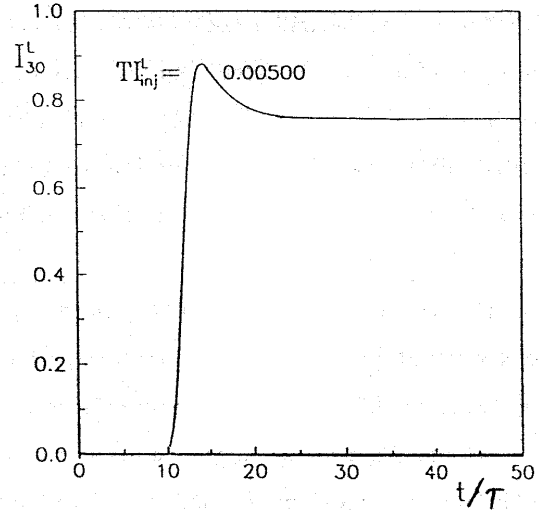


Fig.4: Establishment of oscillation: intensity of oscillating mode  $I_{30}^L$  for real coupling constants  $\gamma_L d = 3$ . Other parameters:  $I_{2d}^L = 1$ ,  $\alpha = 0.5$ .

When the external electric field is present, parameters are mathematically expressed as complex numbers. A typical result of our numerical analysis for mode  $I_{30}^L$  is given in Fig. 5. Graph shape indicates a damped oscillatory behavior of the mode. This behavior could be explained mathematically by the fact that the expression in the exponent of formula (5) is a complex number, which forces periodic characteristics to the considered function.

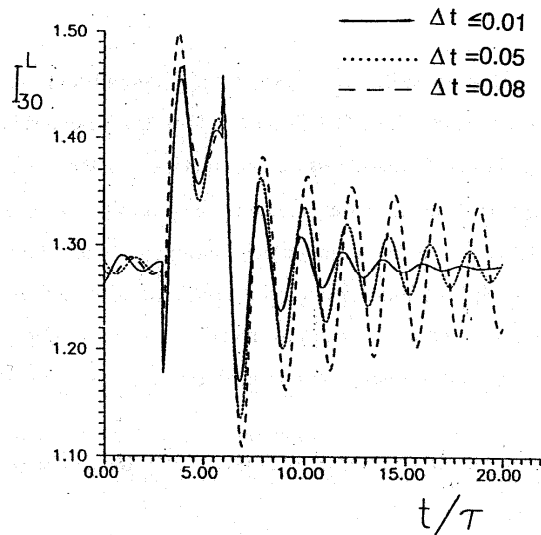


Fig.5: Intracavity field  $I_{30}^L$  as a function of time for different values of the time step. Parameter  $\gamma_L d = 7.07$  and the pump intensity  $I_{2d}^L = 2.22$ .

One can see the difference in the shape of mode  $I_{30}^L$  for this case and for the case when there is no external field (Fig.4).

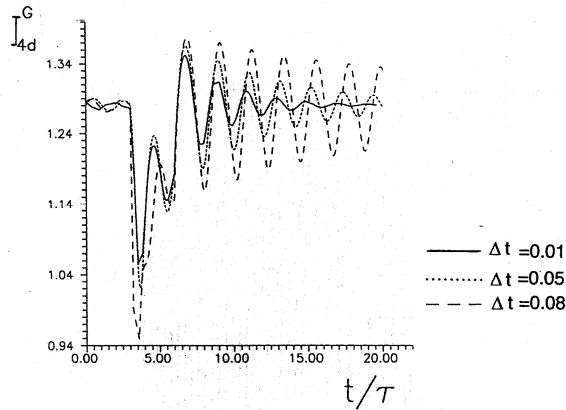


Fig.6: Start of oscillations for the mode  $I_{4d}^G$ , for different values of the time step. The intensities of the corresponding parameters are as in Fig.5.

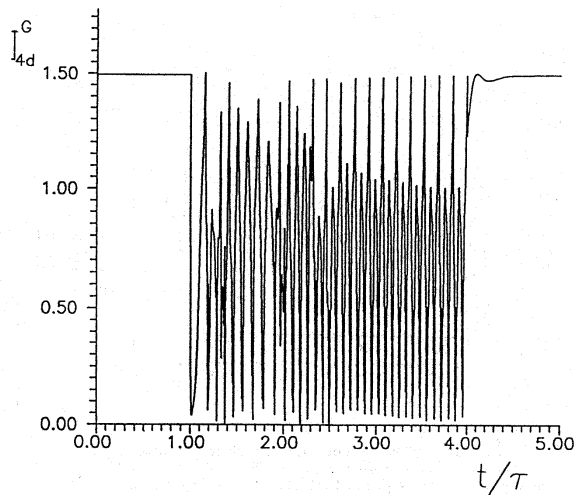


Fig.7: Start of oscillations for the mode  $I_{4d}^G$ . The coupling constant strength is equal to  $\gamma_G d = 21.21$ .

In the graph in Fig.5. one can observe an interesting case of numerical instabilities when choosing the time step for the calculation. The graphs represented with the dashed and dotted lines are not correct, because the time steps have too high values. The graph represented with the solid line is correct, because further decreasing of the time step gives an identical solution. This discussion applies also to the mode  $I_{4d}^G$  (Fig.6.).

In the end, it is necessary to discuss the oscillating modes when the coupling constant has high values (Fig.7.). It was found that the intensities of oscillating modes are then unstable, which means that in this case the flip-flop can not operate.

#### 4. CONCLUSION

Finally, from the all above mentioned we can conclude in general that for the complex values of the coupling constant strength, the flip-flop oscillator can operate. In this case, the oscillating modes show some irregularity in their shape, what is opposite to the case of the modes with the real value of the coupling constant. If the values of the coupling constant strength are too high, the intensities of oscillating modes can not achieve stable states, which means that in this case the flip-flop oscillator can not operate in the stable regime.

#### 5. REFERENCES

- [1] N. V. Kukhtarev, V. Markov and S. Odulov, "Transient energy transfer during hologram formation in LiNbO<sub>3</sub> in external electric field", *Opt. Commun.* **23** 338 (1977).
- [2] M. Belić, "Photorefractive oscillators", unpublished.
- [3] M. Belić and Z. Ljuboje, "Chaos in phase conjugation: physical vs numerical instabilities", *Opt. Quant. Electron.* **24** 745 (1992).
- [4] M. S. Petrović, M. R. Belić, M. V. Jarić, and F. Kaiser, "Optical photorefractive flip-flop oscillator", *Opt. Commun.* **138** 349 (1997).
- [5] Z. Ljuboje, "Oscillating modes of optical flip-flop oscillators in the presence of external electric field", unpublished.

## STRUCTURAL MODELING OF HYDRAULIC SYSTEMS\*

Dragan H. Pršić, Novak N. Nedić, *Faculty of Mechanical Engineering Kraljevo, University of Kragujevac, Serbia and Montenegro*

**Abstract:** *This paper considers the process of structural modeling, in general, and the process of structural modeling based on multiport mechanism, in particular, as base for computer added modeling. This process is illustrated on typical hydraulic control system (cylinder controlled by valve) with systematical approach.*

**Keywords:** structural modeling of physical systems, multiport mechanism, hydraulic control systems.

### 1. INTRODUCTION

The modeling process of a physical systems, in general, could be divide into three abstraction phases [1]:

- physical components phase
- physical concept phase
- mathematical phase

Each of these phases gives some view on a physical system having successful modeling process. Hierarchical structure of this process intensify level details from the level of physical components to the mathematical level. Modeling process begins with recognition of technical components and their interactions into the system to be modeled. This process is basically unique and it is base for the next step. The second step is not unique and it depends from modeling aim and physical concept. This modeling level gives qualitative description of a physical system. The last step is quantitative mathematical description of a physical system and that description can be represented by different mathematical forms.

Structural approach points at possibility to the levels formalization in order to have base for the computer support.

Illustration of these modeling levels, using concept of multiport mechanisms, on hydraulic control systems will be subject of this work.

### 2. ABSTRACTION ON PHYSICAL COMPONENTS PHASE

Introduction with a system (either it is designed or to be designed) begins with establishment of the system's components and their interactions. For graphical system representation could be used non-formal notation or more often domain depended symbols, as in case of hydraulic control system shown in Fig.1.

Given hydraulic scheme represents the first abstraction modeling level (level of physical components). The system composes: hydraulic pump, valve, hydraulic two-way cylinder, reservoir and transmission lines.

This modeling level includes interface between each system's component and the outside world. This is very

important because it helps designer to change any component without the structure destroying. The interfaces on this level are realized by connections (black square in Fig.1). For example, the interface of the hydraulic cylinder composes three connections (Table T1.).

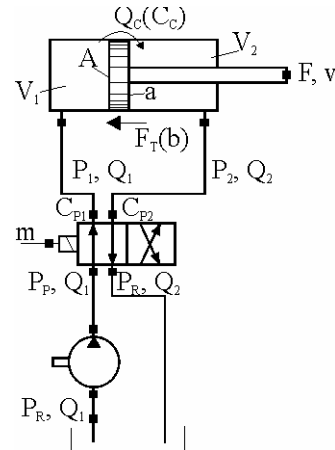


Fig.1: Hydraulic system

Table 1. Hydraulic cylinder interface

Connection		
Number	Domain	Type
1.	Hydraulic ( $P_1, Q_1$ )	Energy
2.	Mechanical ( $F, v$ )	Energy
3.	Hydraulic ( $P_2, Q_2$ )	Energy

Since, looking from outside, hydraulic cylinder we see through interface by three connections it allows substitution of this cylinder by one without interface change.

Each connection represents some kind of component interaction (energy/information) with outside world (model infrastructure). This allows that system can be considered as components net with each other interactions.

### 3. ABSTRACTION ON PHYSICAL CONCEPTS PHASE

Since decomposition of the system into components is ended, the second modeling level begins. Here, to the each component is associated corresponding physical concept which describes it's behavior. The process is not unique and it depends from what is the model aim, that is, it depends from what which physical mechanism going to be associated to component (friction, leakage, stiffness, etc.). Because, this modeling step is the most critical in the all modeling process. The process is very creative and not easy for automation.

For concept qualitative description on this level we use

\* This work is supported by Ministry of Science and Technology of the Republic of Serbia, Project MIS 0090

methodology of the reference approach (RP) [2]. This methodology integrates lumped parameters ontology and energy based ontology by multiport mechanism (Fig.2).

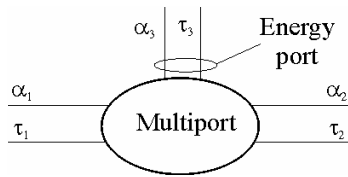


Fig. 2: Multiport mechanism

Energy concept is one of the most important concept in physics. The system mechanical behavior is result of energy exchange between subsystems. This concept is domain invariant and it is good base for system multidomain modeling.

Concept multiport mechanism represents energetic process abstraction and it's interaction with environment. The interaction is represented by conceptual interface which is realized by power port. The ports are places throw energy input and/or output from system and throw them the connection with other mechanism is realized. To each port is associated with two complementary and observable physical quantities  $\alpha$  and  $\tau$ , the product of which is power:

$$P = \alpha\tau.$$

These two quantities ( $\alpha$  and  $\tau$ ) are in generic terms referred to as across (two-point) and through (one-point) quantities respectively.

This across-through distinction of power quantities is based on how the quantities are observed or measured in real world systems. The across type quantities are expressed as differences, and are observed across two spatially different points. On the other hand, the complementary through quantities are observed at one single point.

Example of some across and through quantities in different physical domains are given in Table T.2.

Table T2. Across and through quantities

Domain	Across quantities $\alpha$	Through quantities $\tau$
Mechanical	Force [N]	Velocity [m/s]
	Torque [Nm]	Angular Velocity [rad/s]
Electric	Voltage [V]	Current [A]
Hydraulic	Pressure [Pa]	Volumetric flow [m <sup>3</sup> /s]
Thermodynamic	Temperature [K]	Entropy flow rate [J/Ks]

It could be noticed that ports on the abstraction level correspond to connectors on physical level.

We will now introduce the element mechanisms correspond to basic energetic process (Table T3).

Table T3. The basic multiport mechanisms

Element mechanisms		Interaction mechanisms
Source	$S_\alpha$ $\alpha$ - type	$\alpha$ - distributor
	$S_\tau$ $\tau$ - type	$\tau$ - distributor

Storage	C $\alpha$ - type	
	I $\tau$ - type	
Dissipation	R	
Conversion mechanism	TF Transformer	
	GY Gyrator	

Therefore, the lumped parameter model can be represented as a network of interconnected energetic primitives.

From above, we can see that between the multiport mechanism and element mechanism there is some hierarchical relation. This relation is based on element mechanisms and interaction mechanisms and it provide to keep model structure. Element mechanism is transformed into component and interaction mechanism into connection topology ( $\alpha$ - distributor into parallel connection,  $\tau$ - distributor into serial connection).

Using reference approach syntax, we will determine model of hydraulic system (Fig.1.) based on components model and their connection following structure of the real system.

Starting with the model of variable hydraulic orifice as functional and structural valve divider part, that model is given by Fig.3.

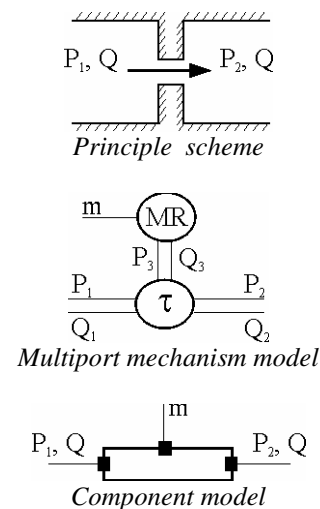


Fig. 3: Model of variable hydraulic orifice

As, in general case, hydraulic resistance can be variable, the orifice is modeling as the modulated dissipator (MR). Modulation can be seen as energetic interaction with neglected flow energy. This means that on one energetic port (modulated port) one of power quantities is approximately zero, but it is not case for another modulated quantities. In such case, energetic flow is neglected, but influence of modulated quantities on other quantities is not neglected.

Now, we can, base on above, to make valve divider model. Assuming the inside leakage, the valve divider model is as shown in Fig.4. [3].

If we not assuming inside leakage, the valve divider model is as shown in Fig.5.

From above, we can see how different physical mechanisms can be introduced in consideration by supplement according energetic concept. This is very important possibility in developing software tool for

computer modeling support.

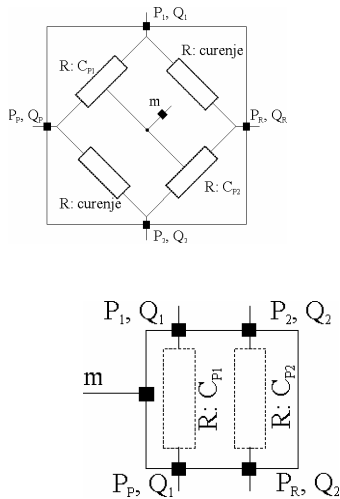


Fig. 4: Valve divider component model with the inside leakage

Fig.5: Valve divider component model without the inside leakage

It is interesting to observe that in both valve divider models ( Fig.4. and Fig.5.), the interface to environment is the same.

Hydraulic cylinder mechanism from Fig.1. (3-port mechanism) will be modeled based on two models: chamber and piston. Hydraulic chamber model for this case is obtained after determination of the generic chamber model. Generic chamber model is shown in Fig.6.

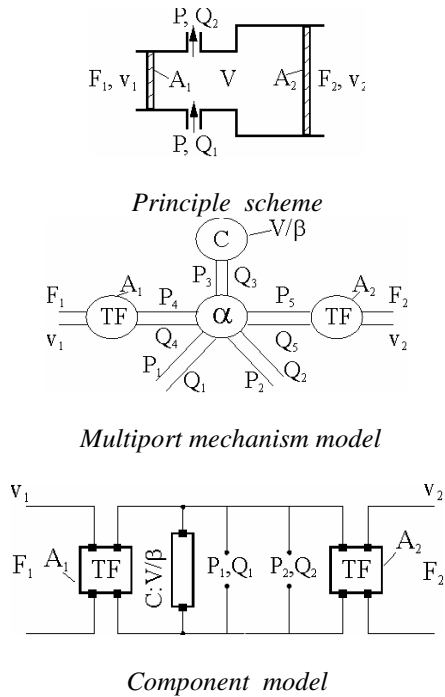


Fig.6: Generic hydraulic chamber model

The piston model is shown in Fig.7.

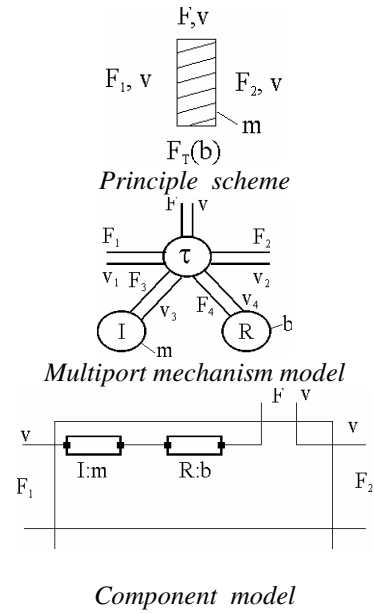


Fig.7: Generic hydraulic piston model

Composing the models of chamber, piston and orifice for the hydraulic cylinder is obtained model (Fig.8).

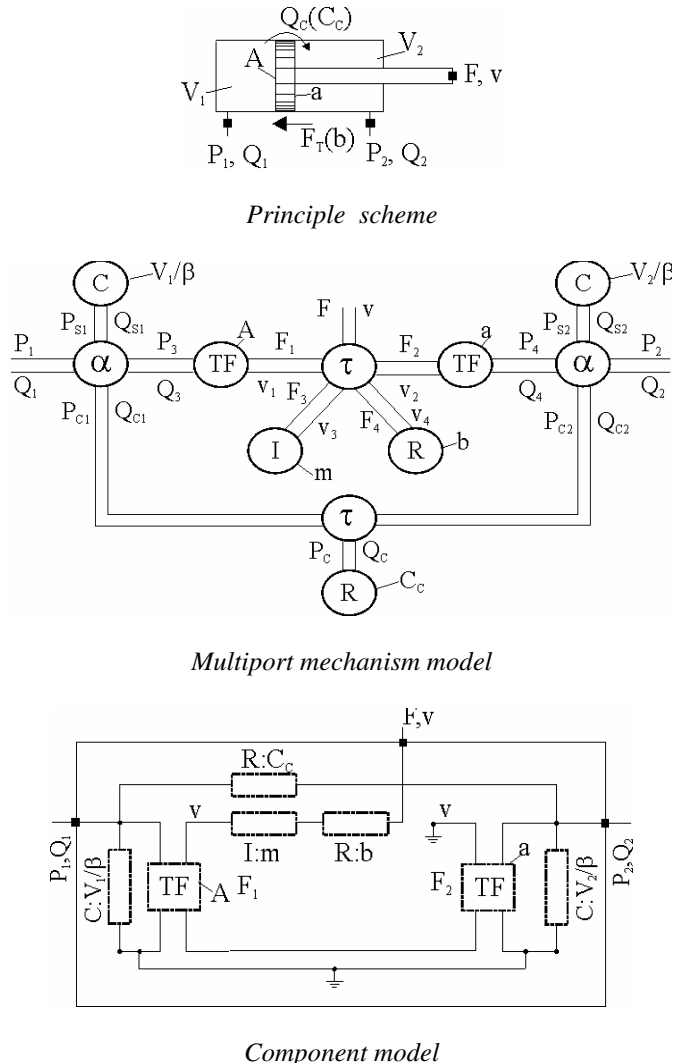


Fig. 8: Hydraulic cylinder model

The pump is assumed as source mechanism ( $\alpha$  - type) and component model is given in Fig.9.

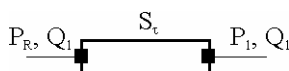


Fig.9. Pump component model

Composing all model components with following the structure of the system it is obtained the component model of the system (Fig.10).

The above given physical model of the system represents some interpretation of the mathematical model, as will be shown by next.

#### 4. MATHEMATICAL ABSTRACTION PHASE

In order to have qualitative system analyses it is necessary to define mathematical relations (variables, constants, parameters) which describe physical mechanisms from previous phase. These relations are denoted as constitutive relations. And while the physical modeling process is creative, the work that demands knowledge and experience, mathematical modeling process can be done by following some algorithm, that is, it can be automated. Acknowledge to that, software tool for computer modeling support become very useful. The model designer can be focused on choice of physical concepts. Otherwise, the work of transfer to mathematical relations become computer work.

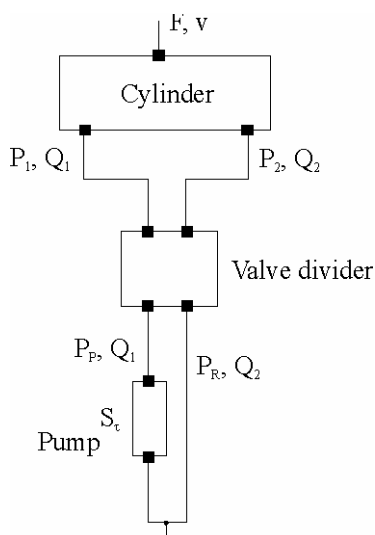


Fig. 10: Hydraulic system component model

Procedure for transfer from conceptual model to mathematical model can be found in [2,4], that is, the next tools can be used: 20-sim, Bondsim, Modelica, etc.

In general, the mathematical abstraction process can be divided into two steps [2]:

1. Definition of constitutive relations for
  - component mechanisms
  - interaction mechanisms
2. Mathematical causalities determination

Relations for component mechanisms depend from

mechanisms characteristics and desired accuracy. First, for each component port couple of quantities that determined energetic flow should be defined. Then, the relation between these quantities should be defined. As, for each energetic primitive is defined constitutive relation the process is algorithmical.

Constitutive relations of hydro cylinder are given in Table T4.

Table T4. Hydro cylinder constitutive relations

Mechanism	Component	Power variables	Constitutive relations
Dissipation	$R: C_c$	$\{P_c, Q_c\}$	$P_c - \frac{1}{C_c} Q_c = 0$
Dissipation	$R: b$	$\{F_4, v_4\}$	$F_4 - b v_4 = 0$
Storage	$C: V_1 / \beta$	$\{P_{S1}, Q_{S1}\}$	$P_{S1} - \frac{\beta}{V_1} \int Q_{S1} dt = 0$
Storage	$C: V_2 / \beta$	$\{P_{S2}, Q_{S2}\}$	$P_{S2} - \frac{\beta}{V_2} \int Q_{S2} dt = 0$
Storage	$I: m$	$\{F_3, v_3\}$	$v_3 - \frac{1}{m} \int F_3 dt = 0$
Transformer	$TF: A$	$\{P_3, Q_3\}$ $\{F_1, v_1\}$	$P_3 - \frac{1}{A} F_1 = 0$ $\frac{1}{A} Q_3 - v_1 = 0$
Transformer	$TF: a$	$\{P_4, Q_4\}$ $\{F_2, v_2\}$	$P_4 - \frac{1}{a} F_2 = 0$ $\frac{1}{a} Q_4 - v_2 = 0$

Interaction mechanism relations are determined on topology connections base and for cylinder are given in Table T5.

Table T5. Constitutive relations of cylinder interaction mechanism

Interaction mechanism	Constitutive relations
$\alpha$	$P_1 = P_{S1} = P_{C1} = P_3$ $Q_1 - Q_{S1} - Q_{C1} - Q_3 = 0$
$\tau$	$F_1 - F_3 - F_4 - F_2 - F = 0$ $v_1 = v_3 = v_4 = v_2 = v$

Should be noticed, that constitutive relations are given in declarative way, not as assign statements. This intensify flexibility and possibility of repeat use of the model. Component model is observed as autonomous model with independent characteristics from working environment [5,6]. In the next step of mathematical modeling, depending of the context model application, we have definition calculation order of constitutive relations. Using procedure RefSCAP [2] we are coming to causal mathematical model (given in form of block diagram) of the hydraulic cylinder (Fig.11).

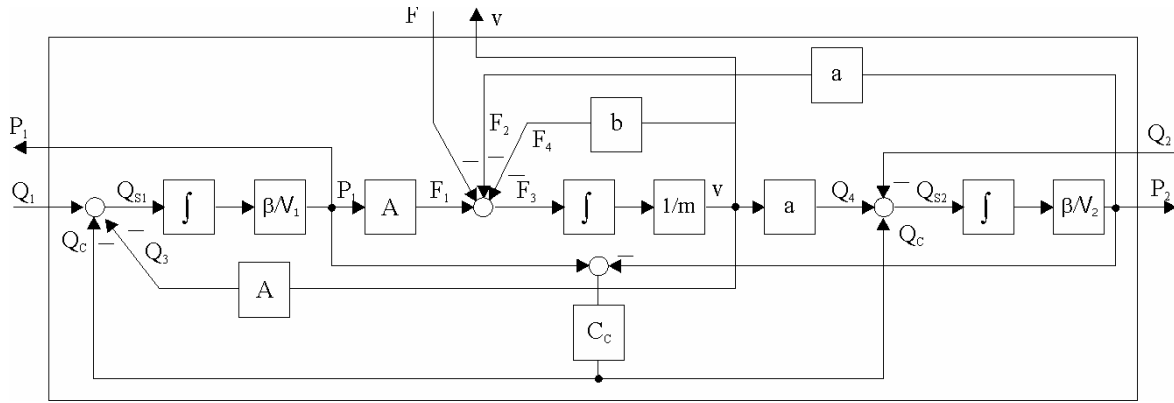


Fig. 11. Block diagram of hydraulic cylinder mathematical model

## 5. CONCLUSION

Here is given methodology of structural modeling of physical system, and it is illustrated on example of hydraulic control system. This structurality is based on hierarchy of modeling process. This process is natural, intuitive and is analogical to hardware system composition. From end user point of view the abstraction level is smaller. The user sees system through physical concept and uses real systems terms. From software tool point of view, transfer from physical to mathematical model is possible by computer support. This allow designer to use his knowledge and experience for more creative work (physical solution problem). Otherwise, computer supports mathematical solution problems .

## 6. REFERENCES

- [1] A.P.J. Breunese et. al., *Libraries of reusable Models: Theory and Application*, Simulation, 71, pp 7-22, 1998.
- [2] Ulf Söderman, *Conceptual Modelling of Physical*

*Systems - a frame of reference*, <http://citeseer.nj.nec.com/373226.html>

- [3] B. Eryilmaz, B. Wilson, *A Unified Model of a Proportional Valve*, Proceedings of the ASME Fluid Power Systems and Technology Division, Nashville, TN, November 1999.
- [4] D. Antić, V. Nikolić, *Contribution to the Conversion of Bond Graph Models into State Space Equations and Block Diagram Simulation Models*, Monographical Booklets, Budapest 2002.
- [5] D. Pršić, N. Nedić, *Object oriented modeling of Hydraulic Systems*, VII International SAUM Conference on Systems, Automatic Control and Measurement, Vrnjačka Banja, Sept. 26-28. 2001.
- [6] D. Pršić, N. Nedić, *Modeling of hydraulic systems using object-oriented language Modelica*, (On Serbian) Infoteh 2002, Jahorina, 2002.

## AN ALGORITHM FOR OFF-NOMINAL FREQUENCY MEASUREMENTS IN ELECTRIC POWER SYSTEMS

*Milenko B. Đurić, Željko R. Đurišić, Faculty of Electrical Engineering  
University of Belgrade, Serbia and Montenegro*

**Abstract:** *Some power system protection applications require accurate estimates of voltage magnitude and frequency over a wide measurement range. Most digital techniques for measuring frequency have acceptable accuracy over a small range in the neighborhood of the nominal value. This paper describes a new algorithm for measuring the frequency in electric power systems. The algorithm is based on the least error squares (LES) technique and uses digitized samples of voltage at a relay location. Mathematical development of the algorithm is presented and the effects of key parameters, that affect the performance of the algorithm, are discussed. The algorithm proposed is the improved version of algorithms developed in References [2, 3, 4]. In this paper, the proposed algorithm is compared with the algorithms from these references.*

**Keywords:** *Power system protection, Frequency measurements, Least error squares methods, Relaying algorithm.*

### 1. INTRODUCTION

Frequency is an important operating parameter of a power system. In the steady state operation of a power system, the total power generated is equal to the system load plus the losses. During operation under such conditions, the system frequency is constant. Generation-load mismatches cause the system frequency to deviate from its nominal value. If the load exceeds the generation, the frequency decreases; if the generation exceeds the load plus the losses, the frequency increases. Underfrequency and overfrequency relays are used to detect these conditions and disconnect load blocks to restore the frequency to its normal value and protect generators from overspeeding.

The algorithms developed [2, 3, 4] are modified here and the introductory analysis is omitted for the sake of brevity. The authors have repeated the calculations with the algorithms proposed in the references cited and the results obtained match the cited results with accuracy. However, the algorithms appeared unreliable when applied to the power system networks where the voltage signal often appears as a distorted one, saturated with the higher harmonic components, ranging from third to eleventh order. When the original algorithms [2, 3, 4] were tested on such a signal, even the small content of higher harmonics, from 3 to 8 %, was the cause of the big errors. In order to minimize the errors introduced by the presence of higher harmonics in the voltage signal, the utilization of the low-pass filters became necessary with these algorithms.

The basic idea of this paper is to modify the voltage signal and thus improve the performance of the filters used in the already existing algorithms [2, 3, 4]. The main purpose was to design the filter that could easily adopt the arbitrarily shaped voltage signal occurring in real power system network and make the new algorithm both sufficiently accurate and relatively simple.

### 2. THE ALGORITHM

This section presents the algorithm which measures the frequency of a voltage signal. It assumes that the system frequency does not change during the data window used for measurement. The algorithm is developed using the (LES) approach and uses digitized values of the voltage sampled at the relay location.

The slightly distorted voltage signal is acquainted in the power system steady state operation and its source is either the power transformer operating on higher than rated voltages or AC/DC converters with thyristors. Let us assume the following observation model of the measured signal, digitized at the relay location:

$$v(t) = V_0 + \sum_{k=1}^M V_k \sin(k\omega t + \theta_k) + e(t).$$

The use of the well known trigonometric identities leads to the following equation

$$v(t) = V_0 + \sum_{k=1}^M V_{rk} \sin(k\omega t) + \sum_{k=1}^M V_{ik} \cos(k\omega t) + e(t) \quad (1)$$

Where:

$v(t)$  - is the instantaneous voltage at time  $t$ ,

$V_0$  - is the magnitude of the DC offset,

$M$  - is the highest order of the harmonic component present in the signal,

$\omega$  - is the fundamental radian frequency of the system in the data window (it is assumed that the frequency does not change during a data window used for measurement).

$V_k$  - is the peak value of the  $k$ -th harmonic component,  $V_{rk} = V_k \cos \theta_k$  and  $V_{ik} = V_k \sin \theta_k$  - are real and imaginary components of  $k$ -th harmonic component,

$\theta = \arctg(V_{ik}/V_{rk})$  - is the phase angle of the  $k$ -th harmonic component and

$e(t)$  - is the zero mean random noise.

The functions  $\sin(k\omega t)$  and  $\cos(k\omega t)$  can be expressed by their first three terms of the Taylor series expansions in the neighborhood of the nominal frequency  $\omega_0$  as

$$\begin{aligned} \sin(k\omega t) &\cong \sin(k\omega_0 t) + \Delta\omega k t \cos(k\omega_0 t) - \\ &- \Delta\omega^2 \frac{k^2 t^2}{2} \sin(k\omega_0 t) \end{aligned} \quad (2)$$

and

$$\begin{aligned} \cos(k\omega t) &\cong \cos(k\omega_0 t) - \Delta\omega t \sin(k\omega_0 t) - \\ &- \Delta\omega^2 \frac{k^2 t^2}{2} \cos(k\omega_0 t), \end{aligned} \quad (3)$$

where  $\Delta\omega = \omega - \omega_0$  is the radian frequency deviation.

After retaining the first three terms of (2) and (3) for fundamental harmonic and first two terms of (2) and (3) for higher harmonics, the substitution into (1) yields:

$$\begin{aligned} v(t) &= V_0 + \sum_{k=1}^M [V_{rk} \sin(k\omega_0 t) + V_{rk} \Delta\omega t \cos(k\omega_0 t)] + \\ &+ \sum_{k=1}^M [V_{ik} \cos(k\omega_0 t) - V_{ik} \Delta\omega t \sin(k\omega_0 t)] - \\ &- V_{r1} \Delta\omega^2 \frac{t^2}{2} \sin(\omega_0 t) - V_{i1} \Delta\omega^2 \frac{t^2}{2} \cos(\omega_0 t) + e(t). \end{aligned} \quad (4)$$

Equation (4) can be rewritten in the abbreviated form as

$$v(t) = \sum_{k=1}^{4M+3} a_j(t) x_j + e(t), \quad (5)$$

Where:

$$\begin{aligned} a_1 &= 1 & x_1 &= V_0 \\ a_2 &= -\frac{t^2}{2} \sin(\omega_0 t) & x_2 &= V_{r1} \Delta\omega^2 \\ a_3 &= -\frac{t^2}{2} \cos(\omega_0 t) & x_3 &= V_{i1} \Delta\omega^2 \\ a_{3+k} &= \sin(k\omega_0 t) & x_{3+k} &= V_{rk} \\ a_{M+3+k} &= kt \cos(k\omega_0 t) & x_{M+3+k} &= V_{rk} \Delta\omega \\ a_{2M+3+k} &= \cos(k\omega_0 t) & x_{2M+3+k} &= V_{ik} \\ a_{3M+3+k} &= -kt \sin(k\omega_0 t) & x_{3M+3+k} &= V_{ik} \Delta\omega \\ k &= 1, \dots, M \end{aligned} \quad (6)$$

If the signal  $v(t)$  is uniformly sampled with the frequency rate  $f_s = 1/T$  Hz during a finite period of time (called data window), one can define a measurement window  $[v]$  as a set of  $m$  consecutive samples ( $m > 4M+3$ ). This set determines  $m$  linear equations in  $4M+3$  unknowns and can be written in the following matrix form:

$$[v] = [a][x] + [e] \quad (7)$$

where  $[v] = [v_1 \ v_2 \ \dots \ v_m]^T$  is an  $(m \times 1)$  measurement vector,  $[a]$ -an  $(m \times (4M+3))$  coefficient matrix, with the elements defined by equations (6) or (8) (in (8) the time is discretized -  $t = nT$ ):

$$a_1(n) = 1,$$

$$\begin{aligned} a_2(n) &= -\frac{(nT)^2}{2} \sin(\omega_0 nT), \\ a_3(n) &= -\frac{(nT)^2}{2} \cos(\omega_0 nT), \\ a_{3+k}(n) &= \sin(k\omega_0 nT), \\ a_{M+3+k}(n) &= knT \cos(k\omega_0 nT), \\ a_{2M+3+k}(n) &= \cos(k\omega_0 nT), \\ a_{3M+3+k}(n) &= -knT \sin(k\omega_0 nT), \\ n &= 1, 2, \dots, m. \end{aligned} \quad (8)$$

$[x]$  is an  $(4M+3) \times 1$  state vector, with the elements defined by equation (6) and  $[e]$  is an error vector, to be minimized.

The elements of matrix  $[a]$  depend on the time reference  $t$  and the sampling rate, and  $T$  can be preselected in an off-line mode. Also, all the elements of  $[x]$  are unknown and functions of  $V_{rk}$ ,  $V_{ik}$ ,  $\omega$ ,  $\omega_0$  and  $V_0$ . To determine the  $(4M+3)$  unknowns of equation (7), at least  $(4M+3)$  equations must be established. In other words, at least  $(4M+3)$  samples of voltage would be required. As a general case, we assume that  $(m)$  samples are available, where  $(m) > 4M+3$ ; then equation (7) describes an overdetermined system. The (LES) technique is used to solve this equation. A complete description of this algorithm is given in [2,3 and 4]. Applying the LES technique on (7) the following result is obtained:

$$[x]^* = \{[a]^T [a]\}^{-1} [a]^T [v] = [A][v],$$

where the matrix  $[A]$  is the left pseudoinverse of matrix  $[a]$ , and  $[x]^*$  is the optimal or best (LES) estimate of  $[x]$ .

Having the state vector  $[x]$ , the magnitude of the DC offset, amplitudes of harmonic components and fundamental radian frequency of the voltage signal can be estimated as

$$V_0 = x_1, \quad V_k = \sqrt{V_{rk}^2 + V_{ik}^2} = \sqrt{x_{3+k}^2 + x_{2M+3+k}^2}, \quad (9a)$$

$$\Delta\omega = \frac{V_{rk} \Delta\omega}{V_{rk}} = \frac{x_{M+3+k}}{x_{3+k}}, \quad (9b)$$

$$\Delta\omega = \frac{V_{ik} \Delta\omega}{V_{ik}} = \frac{x_{3M+3+k}}{x_{2M+3+k}}, \quad (9c)$$

$$|\Delta\omega| = \sqrt{\frac{x_{M+3+k}^2 + x_{3M+3+k}^2}{x_{3+k}^2 + x_{2M+3+k}^2}}, \quad (9d)$$

$$\omega = \omega_0 + \Delta\omega. \quad (9e)$$

Equation (9b) is not suitable when  $V_{rk}$  is small and equation (9c) is not suitable when  $V_{ik}$  is small. A suitable strategy is to use equation (9d) as the frequency deviation estimation proceeds and either equation (9b) or (9c) for the frequency deviation sign determination.

Equation (7) is valid generally, for the signal model containing the DC component and the first ( $M$ ) higher harmonic components. For example, if the voltage signal model contains the first  $M=11$  harmonic components and the DC component, the number of unknowns in  $[x]$  yields  $4M+3=4\cdot 11+3=47$ . Solving (7) even now does not impose a problem. Practical cases introduce even smaller number of unknowns. If a frequency relay with the main task of measuring frequency in steady state and quasi steady state operation is installed in a power system network, the even harmonics in voltage signal are not existing. In this case, if the voltage signal contains all odd harmonics to the eleventh order, the number of unknowns in  $[x]$  is  $4M_{odd}+3=4\cdot 6+3=27$ .

### 3. IMPROVEMENT OF THE ALGORITHM PRESENTED

Unknown parameters of the signal model are estimated by means of (9a-d). It has been shown in [2, 3, 4] that the performances of the algorithm are determined by the choice of the data window size  $T_{dw}$ , the sampling frequency  $f_s$  and the level of the truncation of the Taylor series expansions of non linear terms. The accuracy of the estimation was fully affected by the actually measured value of the signal frequency. The required accuracy was reached only in a narrow range of the expected frequency. The model was not capable of providing a precise measurement over a wide frequency range, as it is shown in the algorithm testing.

Since the algorithm accuracy has been mainly affected by the previously selected expected frequency (equal to the system nominal frequency: 50 or 60 Hz), i.e., by the off-line calculated pseudo-inverse matrix  $[A]$ , the authors drew the conclusion to iteratively update the matrix  $[A]$  in accordance with the actually estimated frequency deviation. In other words, the model linearized in the neighborhood of one point, in the next iteration is linearized in the neighborhood of the new point, calculated as a function of the frequency estimated in the previous iteration. In the context discussed above, the estimation in the  $p$ -th iteration could be expressed as:

$$[x_p]=[A_p(\omega_{p-1})][v_p] \quad (10)$$

where  $\omega_{p-1}$  is the frequency estimated in the previous, the ( $p-1$ )-st, iteration. Using the estimated state vector  $[x_p]$  and equations (9a-e), one readily obtains the estimates of all unknown signal parameters. On the basis of the frequency deviation estimated, follows the update of the  $[A]$  and the new estimation in the step ( $p+1$ ), i.e.:

$$[x_{p+1}]=[A_{p+1}(\omega_p)][v_{p+1}] \quad (11)$$

where an update is provided by:

$$\omega_p = \omega_{p-1} + \Delta\omega_p \cdot$$

Thus, the algorithm for the voltage or current signal parameter estimation can be now subdivided into the following steps:

1. The initial point  $\omega_0$  selection.
2. Signal samples block  $[v_p]$  acquisition.
3. Pseudo-inverse matrix  $[A_p(\omega_{p-1})]$  and optimal estimation  $[x_p]=[A_p(\omega_{p-1})][v_p]$  calculation.
4. Unknown parameter calculation, on the basis of the state vector  $[x_p]$ .
5. Linearization point update  $\omega_p = \omega_{p-1} + \Delta\omega_p$ .
6. Index increment  $p = p+1$  and go to step 2.

At this stage, useful observations about the algorithm stated are made:

1. The range of the measurement and the accuracy are significantly improved.
2. Matrix  $[A]$  now is time dependent and the computational dured is increased.
3. This algorithm could be applied for a different kind of applications, like load-shedding, load restoration, power system protection, power system control, etc.
4. Since the signal model was established in the extended form, a low-pass filter is now not required.

### 4. THE PROPOSED ALGORITHM TESTING

A pure sinusoidal test signal with the following frequency dependence was generated:

$$f = (45 + 10t) \text{ Hz}, \quad 0 \leq t \leq 1s$$

and processed with the algorithm without iterative procedure [2]. The accurate estimates were obtained only in a very narrow frequency range ( $\pm 0.25$  Hz). Such a narrow measurement range would not satisfy the frequency relaying requirements.

The necessity of the model extension was confirmed by processing test signals distorted by the higher harmonics with "the one-sinusoid model" assumed. The maximum estimation errors that occurred when 3., 5., or 7. harmonic (separately) in the amount pf 0.1 p.u. was superimposed were 0.23, 0.1 and 0.08 Hz respectively. Such an inaccuracy should not be accepted from the point of view of underfrequency relaying.

In the following test, the generated test signal, provided as an input to the algorithm, has the following description in harmonic domain:

- fundamental harmonic 100%,
- the 7-th harmonic 20%,
- the 11-th harmonic 10% and
- DC offset 10%.

Using sampling frequency  $f_s = 1000$  Hz and data window size  $T_{dw} = 0.04$  s the exact fundamental frequency estimates are obtained after few iterative steps. The accuracy of the estimates is independent of the number of harmonics and their magnitudes.

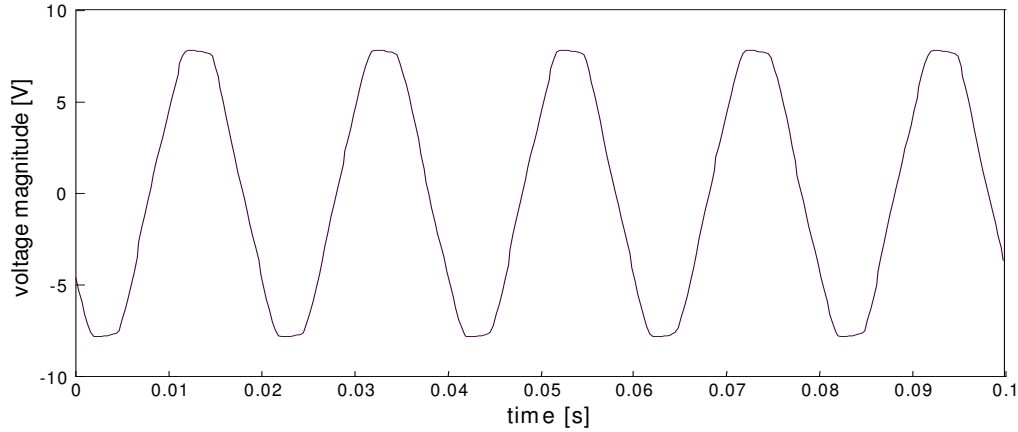


Fig. 1: Recorded voltage signal

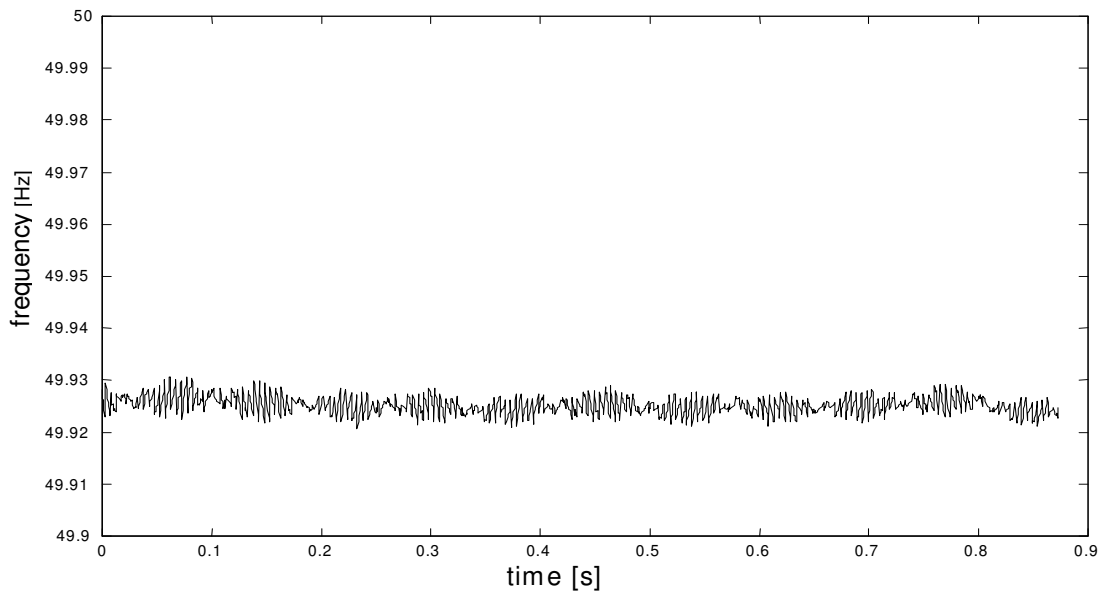


Fig. 2: Frequency estimates of recorded signal

In the following test, the recorded real voltage signal (Fig.1), provided as an input to the algorithm, was used. The result of the frequency estimation with the sampling frequency  $f_s = 1600$  Hz and data window size  $T_{dw} = 0.1$  s is shown in Fig. 2. Exact value of the recorded voltage signal frequency was 49,927 Hz. It is evident that acceptable accuracy was reached using proposed algorithm.

## 5. CONCLUSION

This paper describes iterative digital signal processing algorithm for the frequency estimation of the distorted signals. The algorithm is tested by computer simulations and by processing experimentally obtained data records. It seems to be a very useful tool in the various aspects of power engineering applications, e.g. computer relaying, real-time monitoring and control of system dynamics.

## 6. REFERENCES

- [1] M. S. Sachdev, M. A. Baribeau "A New Algorithm for Digital Impedance Relays", *IEEE Transactions on Power Apparatus and Systems*, Vol. PAS-98, N° 6 Nov./Dec. 1979.
- [2] M. S. Sachdev, M.M. Giray "A Least Error Squares Technique for Determining Power System Frequency", *IEEE Transactions on Power Apparatus and Systems*, Vol. PAS-104, N° 2, February 1985.
- [3] S. A. Soliman, G.S. Christensen, D.H. Kelly, N. Liu "An Algorithm for Frequency Relaying Based on Least Absolute Value Approximations" *Electric Power Systems Research*, 19 (1990) 73-84.
- [4] M. M.Giray, M. S. Sachdev, "Off - Nominal Frequency Measurements in Power Systems", *IEEE Transactions on power Delivery*, Vol. 4, N° 3, July 1989.

## WORKSPACES FOR FUTURE E-SCIENTISTS: GRID AND myGRID

Milena Radenković, School of Computer Science and Information Technology, University of Nottingham, UK

**Abstract:** This paper describes *myGrid* that aims to deliver a personalized collaborative problem-solving platform for e-Scientists working in a distributed environment. It allows them to construct long-lived *in silico* experiments, find and adapt others' experiments, publish their own view in shared repositories, and be better informed as to the provenance of the tools and data directly relevant to them. The focus of *myGrid* is on data-intensive post-genomic functional analysis. The paper motivates the use of GRID as the most effective underlying infrastructure for supporting e-Science applications..

**Keywords:** Grid, myGrid, e-Science.

### 1. INTRODUCTION

Today's science mainly driven by increasingly complex problems and propelled by increasing powerful technology, is as much based on computation data analysis and collaboration as on the efforts of individual experimentalists and theorists. Even though computer power, data storage and communication continues to improve exponentially, computational resources are failing to keep up with what scientists demand of them. The Grid is a new class of infrastructure built on the Internet and the WWW. It provides scalable, secure, high-performance mechanisms for discovering and negotiating access to remote resources and promises to make it possible for scientific collaborations to share resource on a unprecedented scale and for geographically distributed groups to work together in ways that were previously impossible [1].

Although different scenarios vary in complexity, a "Grid"-scenario typically involves several steps: discovering whether remote resources exists, then negotiating access to them, configuring hardware and software to use the resources effectively and doing all this without compromising security of local or remote resources. Implementing these steps requires uniform mechanism for such critical tasks as creating

and managing services on remote computers, supporting single sign on to distributed resources, transferring large datasets at high speeds, forming large distributed virtual communities and maintaining information about the existence, state and usage of community resources.

Grid however goes beyond sharing and distributing data and computation resources. For the scientist the GRID offers new and more powerful ways of working that include:

*Science portals and gateways:* This is usually referred to as "the e-science layer" and aims to isolate the end user (and client software) from the detailed operation and interactions of the core Grid architecture. This layer directly overlays distinctive Grid elements (such as provenance metadata and semantics relationships) on non-Grid services (such as "legacy" Web Services). For example, when accessed through the e-science layer, normal Web Services may appear to expose metadata in a Grid compliant manner when in fact this is being added in transit through the e-science layer. The e-science layer aims to support a diverse range of user interfaces and access devices.

*Computer in the loop instrumentation:* Scientific instruments such as telescopes, synchrotrons and electron microscopes generate row data that are stored for subsequent processing. If scientist could on-demand call on substantial computing resources and sophisticated software, this could greatly enhance instrument capabilities.

*Collaborative work:* Researchers want to aggregate not only data and computing power but also human expertise (i.e. both formal and informal knowledge). Collaborative problems formulation, data analysis and the like are important Grid applications.

Figure 1 illustrates an example deployment perspective for the use of GRID infrastructure emphasising support for heterogenous clients and e-science layer (rather than focusing only on the core GRID that is already illustrated in [1]).

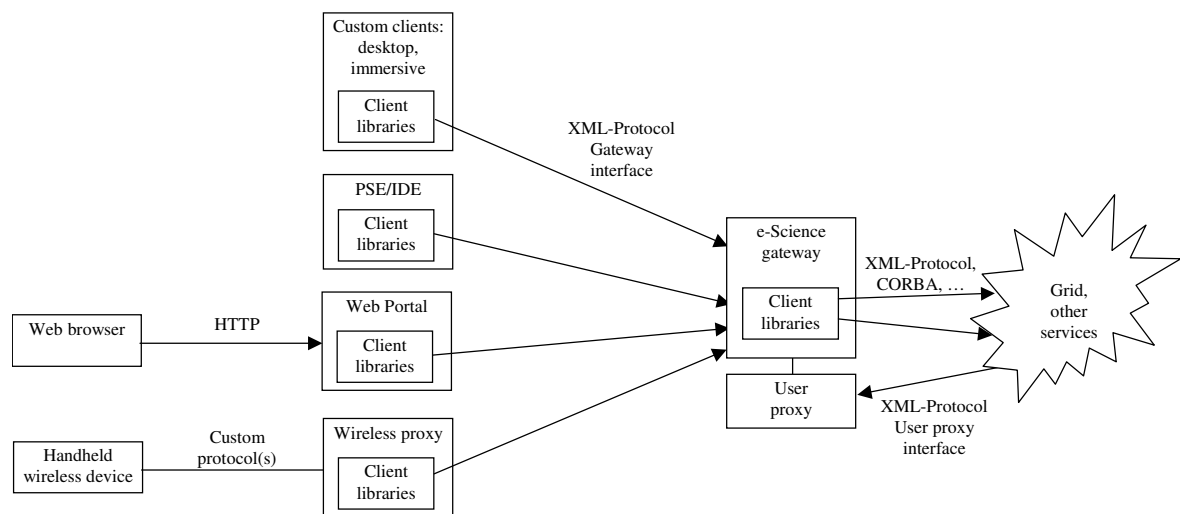


Figure 1 Example scenarios – a deployment perspective

## 2. COMMUNICATIONS IN E-SCIENCE

Almost everything we do involves communications with others. Increasing trend towards collaborative research involves large multi-disciplinary teams, span organisational and geographical boundaries, faster results and more ambitious goals.

Collaboration can be synchronous (e.g. real-time interactions such as virtual laboratories, and on-line conferences, two-way fine grain communications, ad-hoc and unstructured communication patterns, and asynchronous (non real time interaction, course grained communication, more structured communication patterns).

Both forms of communication are required to support flexible collaboration. Persistence and provenance provide basis for asynchronous interactions. User agent/gateway is a persistent representation of the Grid to the user/user to the Grid.

Persistence refers to names, users, services, things, applications and interfaces always being these independent of use or user connectivity. Provenance refers to annotating and relating resources (i.e. data, workflow invocations) to describe derivation, authorship, status, etc

Scientific computing collaborations are often comprised of small teams interacting with other small teams

(large-scale experimental sciences can be much bigger but genome and nanoscience collaborations tend to be smaller [4]). Because they typically involve only a few people and only loose cooperation between different laboratories, the need for real-time cooperative work tools is relatively small and support for collaboration should focus on retrieval and analysis of archival data and literature and on extending the same facilities to more informal material that is crucial to progress in science [4].

Most of the current collaborative toolkits for e-science enable two or more people to access documents, applications, resources and interfaces, as well as interlinked collection of personal and public workspaces. They are usually based only on specific coordination policies and mechanisms (access control and permissions) determine who is permitted to share and how sharing is accomplished. Workflow management and collaborative workflow is currently a hot topic in industry and research. Groupware systems mostly only bundle some basic workflow capabilities that can be used to process workflows. Consequently, there is an alarming need for more sophisticated collaborative toolkits that would allow non-trivial and scalable collaboration among geographically dispersed users.

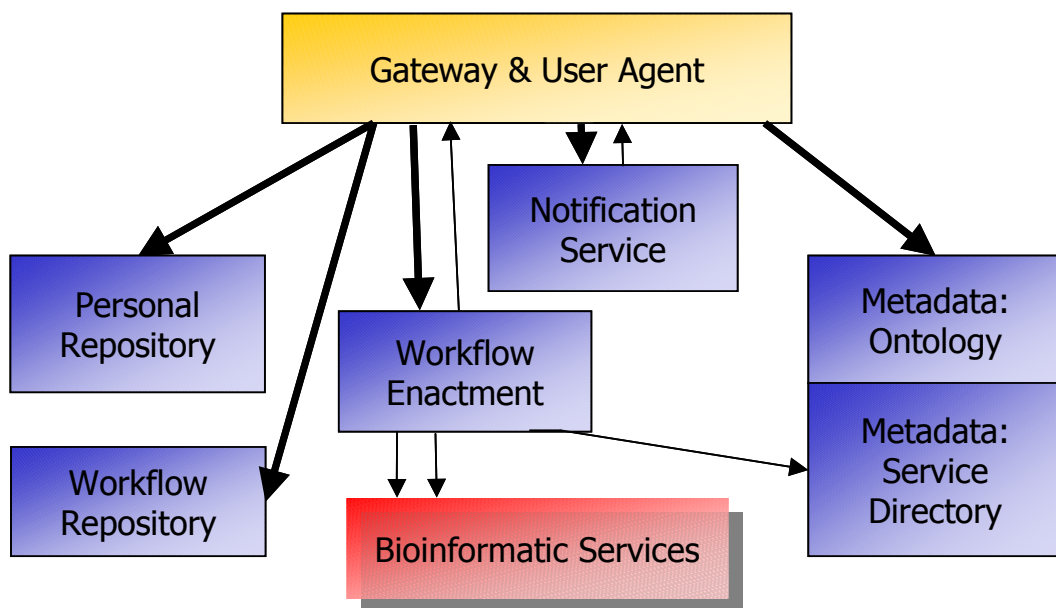


Figure 2 Architectural Overview and interaction in myGrid

## 3. myGRID: ARCHITECTURAL AND COLLABORATION SUPPORT OVERVIEW

MyGrid is a Grid middleware project that aims to help bioinformaticians and biologists to perform workflow-based in-silico experiments and help them automate the management of such workflows through personalisation, provenance and notification of change. In biological sciences it is not the quantity but the complexity of the data that matters [3]. Most biologists have fairly modest requirements for computer power. What is most important to them is discovering resources, discovering tools, and being able to capture when, where, and why [they] did a [certain task]. MyGrid is being developed as a semantically rich layer to sit

on top of a computational Grid infrastructure, and will eventually enable scientists to find and retrieve the data and applications they want. In these environments complex heterogeneous data are under constant change. Term *data* in this context refers to: row data (domain entities, workflow definition), metadata, provenance, annotations, versioning, results, partial results. MyGrid allows large numbers of repositories and tools to be involved in the computation process, complex queries, transparent manipulation of multiple data and metadata sources, suspending and resuming workflows, observing workflow progress, analysing their progress. Figure 2 illustrates high level overview of myGrid

architecture that provides the following functionalities: access (personal and public repositories), domain-specific computational services and service discovery services, workflow enactment engine, notification and metadata services as well as the user agent and gateway services.

Figure 3 illustrates a particular myGrid use case in which user can browse through repositories (list items and workflow executions, view output and other provenance log generated by workflow), locate workflows and run them. In this figure

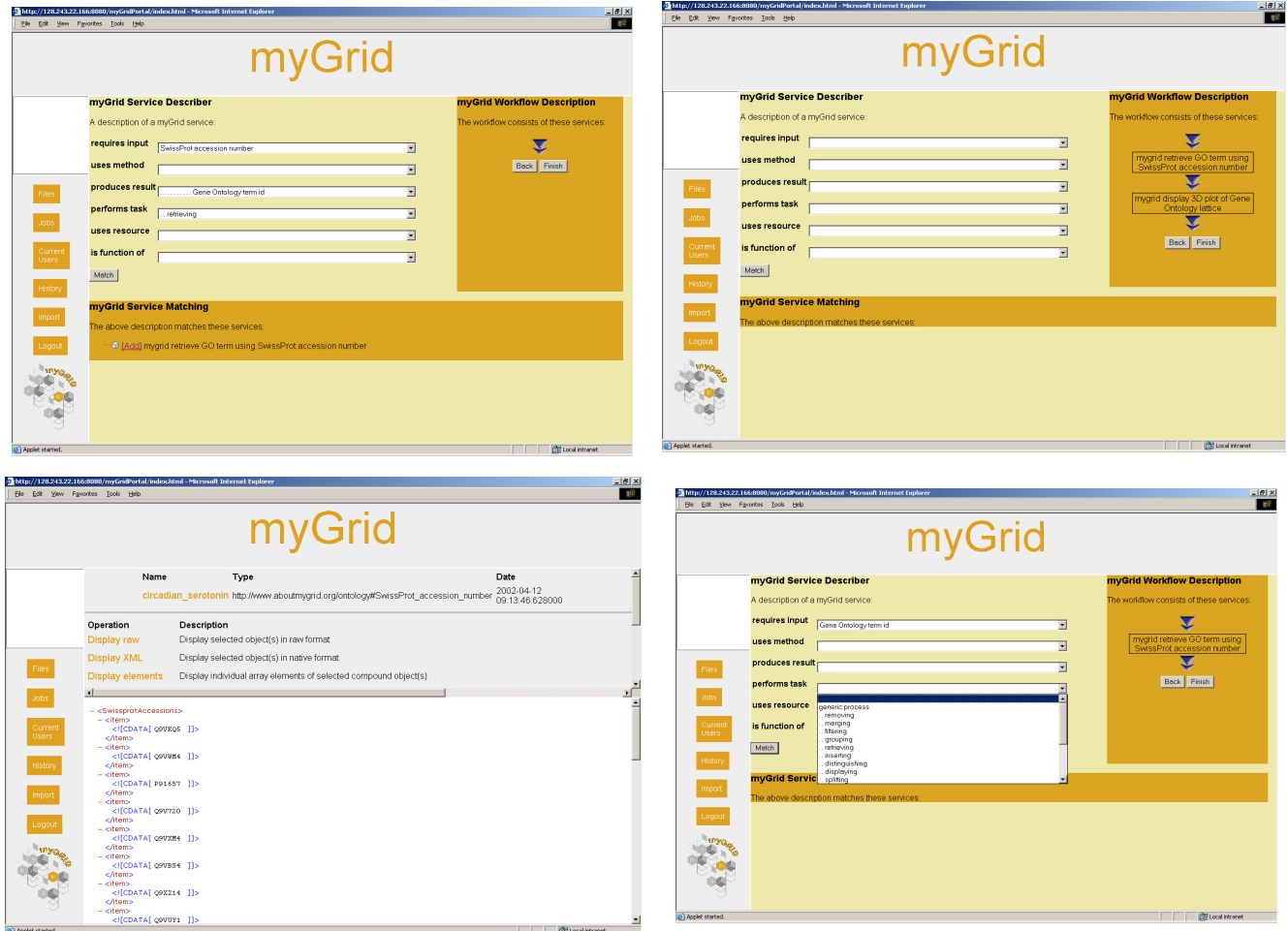


Figure 3 A Scientist browsing repositories and enacting workflows

#### 4. CONCLUSIONS

Even though in its early stages, MyGrid has already been used in a variety of genome academic and industrial research projects as well as in an educational settings. It proved to provide an efficient environment for scientist to collaboratively run their workflows as well as help them share both formal and informal knowledge. Work to date mainly concentrated on designing and implementing generic myGrid infrastructure. Graves' Disease has been selected as the specific application domain for the next integration fest in which myGrid functionality will be demonstrated to myGrid industrial partners as well as wider audience.

#### 5. REFERENCES

[1] Foster and C. Kesselman (Eds.), Morgan-Kaufmann, *The Grid: Blueprint for a New Computing Infrastructure*, 1998

database a user selects an item from the personal repository, identifies an operation class to be applied to the selected item from the ontology service, and then looks up workflows implementing this class of operation from a service directory, and retrieves associated metadata. Based on metadata the user retrieves the specific workflow definition; enacted the workflow using a workflow enactment engine.

Figure 4 illustrates provenance being retrieved after the workflow has finished executions.

- [2] James D. Mayers, Collaborative Electronic Notebooks as Electronic Records: Design Issues for the secure Electronic Laboratory Notebook (ELN), *Proceedings of the 2003 International Symposium On Collaborative Technologies and Systems (CTS'03), January 19-24, 2003, Orlando, Florida*
- [3] Luc Moreau, Simon Miles et al, On the Use of Agents in Bioinformatics Grid, *NETTAB 2002, NETTAB 2002 Bologne, Italy*
- [4] B. R. Schatz, Building Collaboratories for Molecular Biology, *In National Collaboratories: Applying Information Technology for Scientific Research, National Research Council, National Academy Press, Washington, DC, 1993.*

## SPECIAL NOISE REDUCTION DIGITAL FILTERS IMPLEMENTATION<sup>1</sup>

Darko Nikolić, Petar Rajković, Dragan Janković, *Faculty of Electronic Engineering, University of Niš*

**Abstract:** *One of the most important segments of digital picture processing is noise-reduction. Every kind of real problems is characterized by special type of noise. This paper presents results of special noise-reduction digital filters implementation for neutrophil cell analysis and for generating 3D space model from geographic maps. Background elimination and segmentation are implemented for neutrophil analysis, and text elimination (complex noise reduction) and edge converting are realized for 3D modeling. Effects of those filters are presented by this work.*

**Keywords:** *Noise Reduction, Noise Elimination, Digital Filter, Neutrophil Cell Analysis, Background Elimination, Threshold, Segmentation, Granolas, Geographic Map, Generation 3D Model, Digital Image, Digital Picture, Borders, Text, Underlined Text, Elimination of sharp edges between areas with different heights.*

### 1. PREFACE

Noise reduction is one of the most important segments in complex process of digital picture processing. The result of noise reduction is picture that can be easily used for further processing. Depending of solving picture processing problem, definition of noise is different. Once noise is defined, the elimination strategy can be determined.

Otherwise, the noise is not only problem. Excepting noise, there are a lot of practical problems such resolution that is not suitable for processing, used color models etc. The most often used color model is RGB, but in some cases CMYK and HSV are more adequate. In some applications, the right choice of color model can be the main factor for successful realization.

HSV color model, in brief, defines the mean of colors. This is, by some authors, the most natural color model. Its H-component (hue) defines base color, S-component (saturation) level of white that is combined with base color and V-component (value) quantity of emitted light (sharpness of color). This model is proper for application where is most important part of processing mapping light and shadow on picture[1].

The RGB model is the most useful for color picture segmentation. The picture can be segmented by histograms of all of its three channels (Red, Green, and Blue). Segmentation can be implemented on two ways: global and local segmentation. Global segmentation is segmentation applied to whole picture, and local is that applied on one particular area.

Processing of particular components of color can be very important part of image processing. Modification of dependencies between color components results with pictures that can be more useful for further processing. This approach to image processing was used for pictures that represent samples of neutrophil cells. Results of image filtering by this way were very good.

Second part of this paper represents processing of pictures that representing geographic maps. The main part of this processing is elimination of labels from maps. The base for this filter is median filter[1] which is changed a lot for this application. There is implemented variable dimension of window as well as different algorithm of computing target values.

The main purpose of this paper is representing different strategies for solving one problem – noise reduction from digital images.

### 2. USING DIGITAL FILTERS AT NEUTROPHIL CELLS ANALYSIS

Neutrophils are subtype of lymphocyte cells and they are the largest in number of all. The rate of neutrophils in lymphocytes is between 50 and 70%. Their main characteristic is segmented nucleus and cytoplasm with granolas[2].

Figure 2.1 represents system for microscope samples analysis. Optical microscope, digital camera and a computer are the main parts of this system. This system works on following way:

1. digital (CCD) camera transform the picture of microscope sample in some digital image format
2. computer stores created digital picture on disk
3. application processes stored pictures and generates requested results. Image processing, in this case, is very complex job (fig. 2.2).

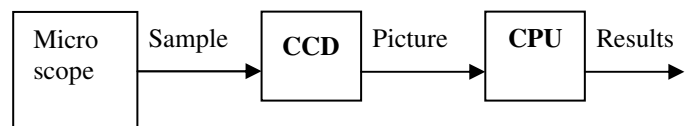


Figure 2.1. *System for microscope samples analysis*

<sup>1</sup> The writing of this paper was partly supported by the MNTR (Project No. IT1.23.0047.A)

Realized application realizes several functionalities: preprocessing of image, background elimination, segmentation, active cell areas localization, measuring cell activity and representing of image processing results. Those results are different reports about analyzed microscope samples as well as processed pictures. All of them can be archived later. This software is developed using Microsoft Visual C++ [3] as Windows application.

The base color model used in this application is RGB model. Channel-independent picture processing is implemented through channel mixer. It allows changing attributes of every channel and relations between them, as well as contrast and sharpness. Dialog of channel mixer is shown on fig. 2.3.

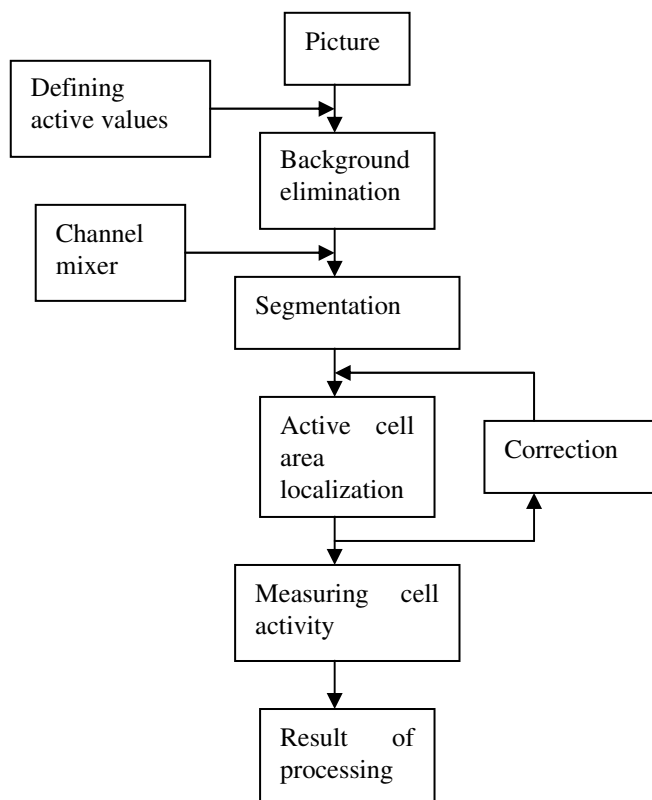


Figure 2.2. *Image processing*

Channel-independent picture processing allows easier active cells detecting. Cells are active if their cytoplasm contains small islands, called granolas. Those granolas are darker than rest of cytoplasm, but not enough. Without changing relations between channels segmentation could not detect both nucleus and granolas. Eliminating red color component, more than blue and green, granolas become more visible and they can be selected easier. Changing the contrast of picture granolas become visible as well as nucleus.

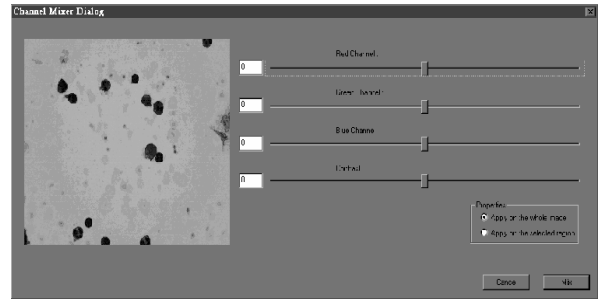


Figure 2.3. *Channel mixer dialog*

After these actions, the most of granolas should be segmented with nucleus, and will create "segmentation mask". This procedure can be done automatically using default values of processing parameters. Default values are set as result of statistical analysis of more than 100 pictures. But, in some cases, changing default values results in better output. The reason for that changing is fact that microscope samples cannot be colored in the same way, because the microscope operator cannot color all of them with same intensity of color. Figures 2.4 and 2.5 show result of described transformation.

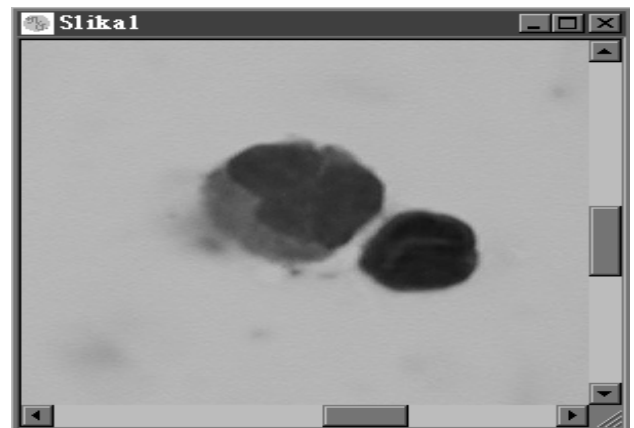


Figure 2.4. *Cells before processing*

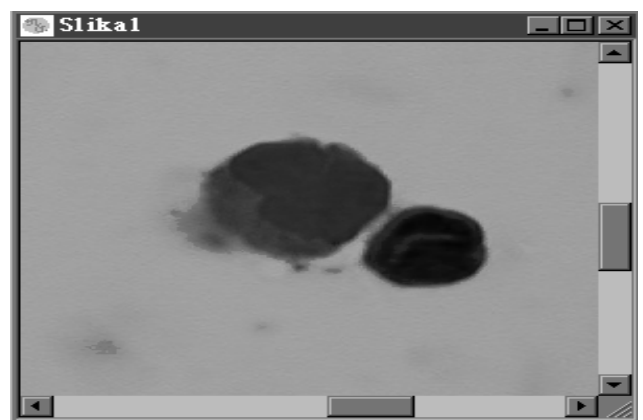


Figure 2.5. *Cells after processing*

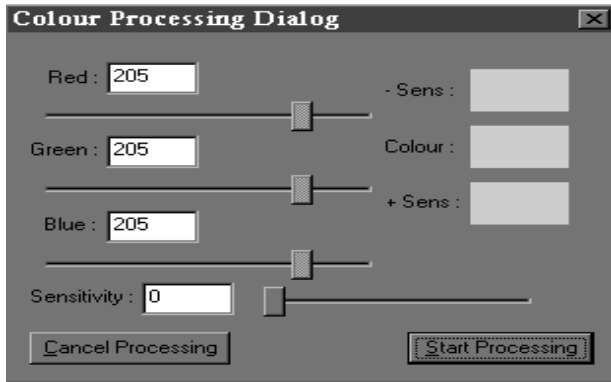


Figure 2.6. *Color processing dialog*

As it can be seen on fig. 2.5. borders of cells and granolas are more expressive. Additional filtering is noise elimination. Noise on this class of pictures is blood plasma as well as the others blood cells. Blood plasma consists of different types of erythrocyte, trombocyte, monocyte and neutrophil cells. On the microscope sample, all of these cells are colored by similar colors, so automatic neutrophil cells detection can detect some of the others. Background elimination reduce this problem very well.

In a lot of cases, background elimination makes visible many characteristics of neutrophil cells. Realized software allows both local and total background elimination. Advantage of local processing is useful for analyzing of some particular area with a single cell. Figure 2.6. shows color processing dialog.

Setting value of parameter *Sensitivity* (Sens in color processing dialog), changing threshold for eliminating background. Wider threshold eliminates more elements from background. But, too wide threshold eliminates some elements of useful objects. So, default threshold values are set experimentally. Effects of background elimination are shown on figures 2.7 and 2.8. This procedure can be used for different filtering during image processing.

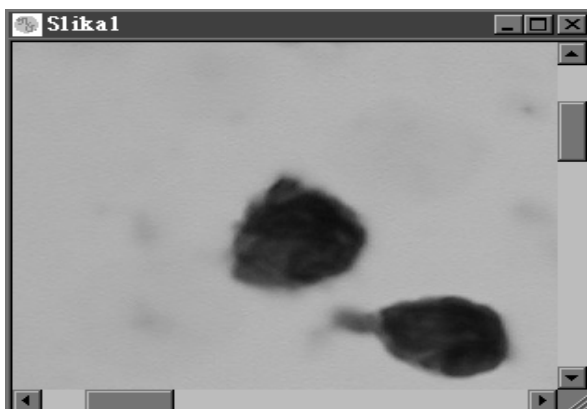


Figure 2.7. *Neutrophil cell on non-uniform background*

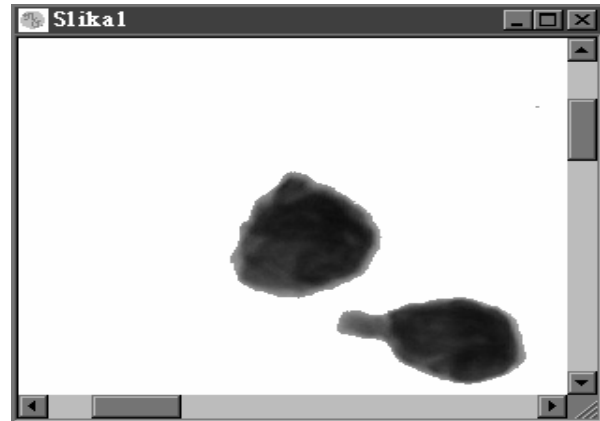


Figure 2.8. *Cells after background elimination*

Segmentation is the last one step in preparing picture for processing and selecting useful objects from picture. The base for segmentation is one of channel histograms of RGB model. Also, this application implements and segmentation for HSV model. First, setting values of threshold should be done. Those values are set by the analysis of the shape of histograms. Minimum of histograms is the best value for threshold. Operations on histograms, such is normalization, can take effect on segmentation, and improve quality of resulting picture.

In this application segmentation is done on two thresholds. Both nucleus and granolas are selected by first threshold (fig. 2.9), but, only nucleus by second (fig. 2.10). Result of eliminating the contents of picture after second segmentation from picture which is result of first is the picture that contains only granolas. Now, counting of active cells (cells with granolas) and computing needed parameters is trivial. The level of error in results is acceptable for all kind of analysis.



Figure 2.9. *Result of first segmentation*



Figure 2.10. Result of second segmentation

### 3. USING DIGITAL FILTERS FOR NOISE ELIMINATION FROM GEOGRAPHIC MAPS

Digital picture processing filters, that are described in following chapter, are used for eliminating all main problems in 3D surface generating process. All of these filters are implemented as part of program called GEO that converts geographic map (bmp, jpg or gif picture) in 3D model of surface. Visualization is realized using OpenGL. Except that, functions, such as rotation, for manipulation with created 3D scene are also implemented. Geographic cards, as digital images, are taken from Encarta's World Atlas.

First step in image processing is noise eliminating. In this case noises are different non-geographic elements on geographic map, such as all kind of text, borders, shadows etc. Eliminating the borders was the most difficult problem, because the color used for their marking was not shades of red but green. Shades of green, that are used for representing borders, are also used, on same picture, for describing relief (lowlands and depressions). But, all of these problems are solved successfully by implemented complex filter.



Figure 3.1. Image before processing

Edge transformation, that eliminates sharp edges between areas with different heights above sea level, is also

realized. Here is implemented an algorithm that is based on calculating height of specific point by statements that include starting value of point's height and distances from its area borders.

Figure 3.2 represents result of filtering picture from figure 3.1 using special filter. That filter work on the following way. Loading picture from a file, filter read it pixel by pixel. Pixels with proper values, elements of surfaces, are written in auxiliary array with adequate values. But, pixels with "wrong" values, noises, are written in same auxiliary array with negative value. Further transformations are done on formed auxiliary array.

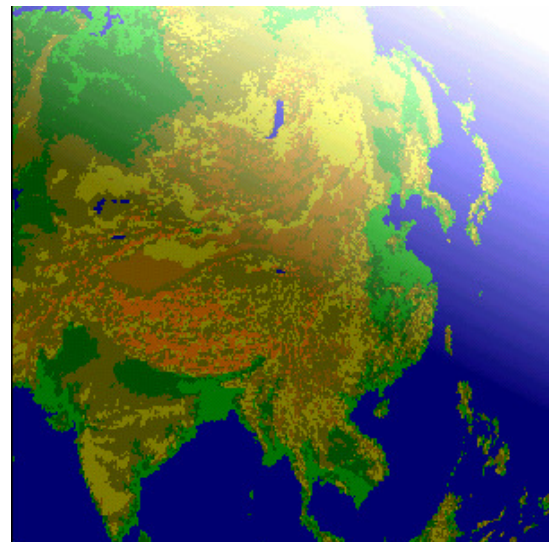


Figure 3.2. Picture from fig. 3.1. after noise elimination

Next step is negative values elimination. When some pixel with negative value is found, its value is changed by some proper value. Filter determinates new value analyzing neighbors of "wrong" pixel. It analyzes neighbor pixels in all eight ways from starting pixel. It analyzes one by one pixel in each way while proper pixels are found. Now, filter replaces negative value by value of found proper pixel. If filter finds more than one proper pixel it replace negative value by the value of last founded. In the process of development of this filter some other strategies for negative value eliminating are considered. All of these methods are much more complex but improving of results is minor.

Using shades of green for representing borders between regions and countries, that are the same like those used for describing lowlands, was the biggest problem. But, there was one good thing: marked borders has same width on every map. So that, one small routine that look up for borders is implemented as a part of complex filter. Now, completely filtered picture can be represented in 3D. Example of 3D scene generated by this way is given on figure 3.3.

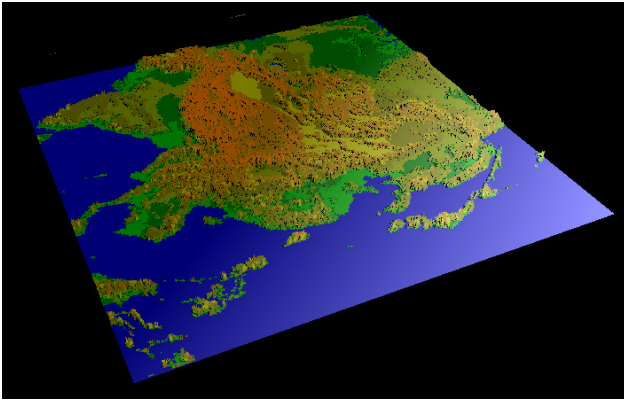


Figure 3.3. 3D scene generated on the base of image represented on figure 3.1

Elimination of sharp edges between areas with different heights is realized implementing an algorithm that is based on measuring distances between point and borders of its area. In this case, term “*area*” describes space that contains points with same height level, and the term “*neighbor*” is used to describe points from the other side of border of area that contains considering point. Every point has 8 neighbors (north, east, south, west, NE, SE, NW, and SW). Algorithm calculate d-value (distance) and h-value (height) for each neighbor, and, using them, calculate new value of height for considering point. Special cases like: what if all the neighbors have same h-value are included in algorithm. Effect of this operation can be seen on figure 3.4.

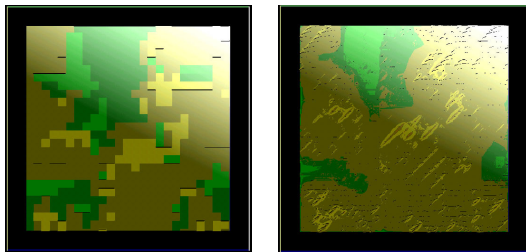


Figure 3.4 Detail of picture under maximal zoom (zoom 32) without (left) and with elimination of sharp edges between areas with different heights above sea level (right)

Noise elimination filter, used for primary transformation of loaded picture, represents a filter with variable size of window. It replace the value of point that is located in its center (considering point) with value of some other point that is element of filter’s window. This filter produces good results on this type of images. All non-geographic and other “*noisy*” elements, like different titles then borders and rivers, are successfully eliminated from loaded picture. Beside this, filter eliminates underlined text too. Elimination of underlined text was the greatest problem in filter realization.

During process of program development, it was experimented with different types of known filters. In the beginning it was used median filter and its modifications, but results were unsatisfied. Because, this type of filter eliminate noise, but, in the same time, change values of valid pixels.

Mentioned problem was the main reason for realizing new filter that is described earlier in the text. The main advantage of our filter are:

1. it does not change values of valid pixels;
2. variable size of window allows adapting of filter’s algorithm for each pixel automatically;
3. implementing code for handling with special cases, filter eliminate all noticed algorithmic errors.

Figures 3.1 and 3.2 show picture before and after filtering.

Three-dimensional scene representation is realized using OpenGL, under Microsoft Visual C++ development environment. Light is positioned on eastern side of scene that makes its look more realistic.

#### 4. CONCLUSION

This paper represents practical realization of different strategies for noise reduction and elimination from digital images. Those strategies are implemented through realization of programs from neutrophil analysis and generating three-dimensional scenes that represents earth’s surface. Both programs are realized like student’s projects for course named “*Pattern recognition*”.

At the system for neutrophil cells analysis there are applied methods for background elimination and threshold segmentation. In this case, threshold segmentation on two thresholds is realized. As a result, this system provides both number of active and non-active cells, as well as numerically quantized cell activity and corresponding tables and charts.

The main parts of the software for 3D visualization are filters with variable size of window that eliminates titles and borders from geographic map and algorithm for elimination of sharp edges between areas with different heights. The base for projected noise-elimination filter were existing filters like median and Gaussian.

Both programs, presented by this paper, that consist parts for noise elimination from digital image, solve concrete image processing problems. The software solutions, made from realization these systems, are very efficient tools for digital image processing and they fulfill all project requests.

#### 5. REFERENCES

- [1] William K. Pratt, *Digital Image Processing*, John Wiley& Sons Inc, New York, 1978.
- [2] Ivan Nikolić, *Ćelije i tkiva*, Medicinski fakultet, Niš, 2002. (on Serbian)
- [3] Ričard Lineker i Tom Arčer: *Visual C++ Biblija*, prevod Mikro knjiga, Beograd 1999.
- [4] World Atlas, taken from: [www.encarta.msn.com](http://www.encarta.msn.com)
- [5] OpenGL Tutorial: <http://www.dev-gallery.com>
- [6] Dragan Urošević: *Algoritmi u programskom jeziku C*, Beograd 1991. (on Serbian)

## SOME POSSIBILITIES OF ARBITRARY WAVEFORM SYNTHESIS FOR DPS SYSTEMS

*Bosiljka Vukčević, Technical College, Beogradska 20, 18000 Nis, Serbia and Montenegro*

**Abstract:** *The paper presents a new hardware architecture for the realization of arbitrary waveform generators. It is based on Look - up tables realized by a dual port RAM. As one of essential building blocks, the paper deals with building blocks of the signal processing system to be used in measurement and control applications.*

**Keywords:** *Arbitrary waveform synthesis, Generator module, Look - up tables.*

### 1. INTRODUCTION

The signal processing block is one of the most important elements in process control systems. Sinusoidal signal generators, as well as arbitrary waveform signal generators play a very significant role in signal processing. Even though a great variety of signal processors dedicated to digital signal processing (DSP) have been developed, there are only two basic methods for realization of sinusoidal and arbitrary waveform generators. One of them is based on exploiting Look - up tables, while the other is based on the on - line calculation of the values.

The first method, based on reading the values from the Look - up table and on the calculation of a more accurate lineally interpolated value that may be due, enables a minimal harmonic distortion, and, consequently, a minimal error. The Look - up table is stored in the corresponding memory space realized as ROM. However, since a separate and independent Look - up table in ROM must exist for every single waveform, the number of waveforms to be generated in this manner is directly limited by the available memory space.

Compared with the first, the second method requires considerably less memory space, and is used for very short programs. However, in case of high - speed signal generation (high frequency signals), this method loses high precision which results in considerable errors. Since the function defining signal waveform is approximated by mathematical series, it is possible to generate an arbitrary number of different waveforms.

### 2. ARBITRARY WAVEFORM SYNTHESIZER MODUL

Look - up tables located in ROM are suitable for the generation of the signals of a specific, let's say, simple periodic form. However, generation of a considerable number of the arbitrary form signals requires an impermissibly large amount of ROM space to store a large number of Look - up tables. On the other hand, calculation of the value of the signal defined by mathematical series or by some other mathematical expression, sets practically no limits as far as the number of different waveform signals is concerned, but fails to provide satisfying accuracy for the allowable time of calculation.

In order to make good use of the advantages of the above methods, as a building block in signal processing systems, a solution is suggested which implies the presence of Look - up tables in ROM space only for the basic signal waveforms. The said values enable sufficiently quick calculation of the values for complex signal forms. Also, for

the increase of resolution - number of samples for conversion, it is possible to calculate the values of the samples with a lesser step using adjoining values from the Look - up table and linear interpolation. The formula to be used for calculations is

$$y = y_i + \frac{x - x_i}{x_{i+1} - x_i} (y_{i+1} - y_i) \quad (1)$$

where  $y_i$  and  $y_{i+1}$  are two adjoining signal values from the Look - up table in  $x_i$  and  $x_{i+1}$ , and  $x$  is the value between them on the time axis.

The architecture of the proposed arbitrary waveform synthesizer modul is shown in Fig. 1.

The reading frequency (fs) of sample values from the Look - up table is determined by a programmable clock generator module. The maximal frequency is limited by the time needed to access DP RAM in order to read it, i.e. by D/A converter setting time. Present - day submicronic technologies used in construction of integrated circuits provides for a Look - up table reading period of several tenths of nsec, i.e. provides for a reading frequency which approximates up to 50 MHz.

A 16 - bit D/A converter provides amplitude signal resolution of:

$$\frac{\Delta V}{V_{pp}} = \frac{1}{64K} \quad (2)$$

For the highest signal amplitudes ( $V_{pp} = 10V$ ) the step of voltage change is  $\approx 0.15mV$ . Module programmable amplifier provides for an opportunity to choose one particular output voltage band out of the available specter. Programmable address sequencer enables setting of start and end addresses of storage locations containing the Look - up table. Upon activating the generation command it provides a cyclic selection of successive locations of the Look - up table. It can be programmed to continue reading from the beginning upon reading the end location of the Look - up table, or to terminate signal generation. The processor is enabled to read the status of the programmable sequencer.

Programming of start and end addresses renders possible to split the memory space into blocks (for instance, 2K locations each), so that each block contains a Look - up table of a preferable waveform signal, or to store the values of the new Look - up table in the other block during the generation - reading of values in the first one (Look - up table).

The glitches appearing in the transition state on the output of D/A converter are eliminated by a Sample/Hold circuit. It samples the output of D/A converter just before a new digital value is set on its input, i.e. when the output is stable.

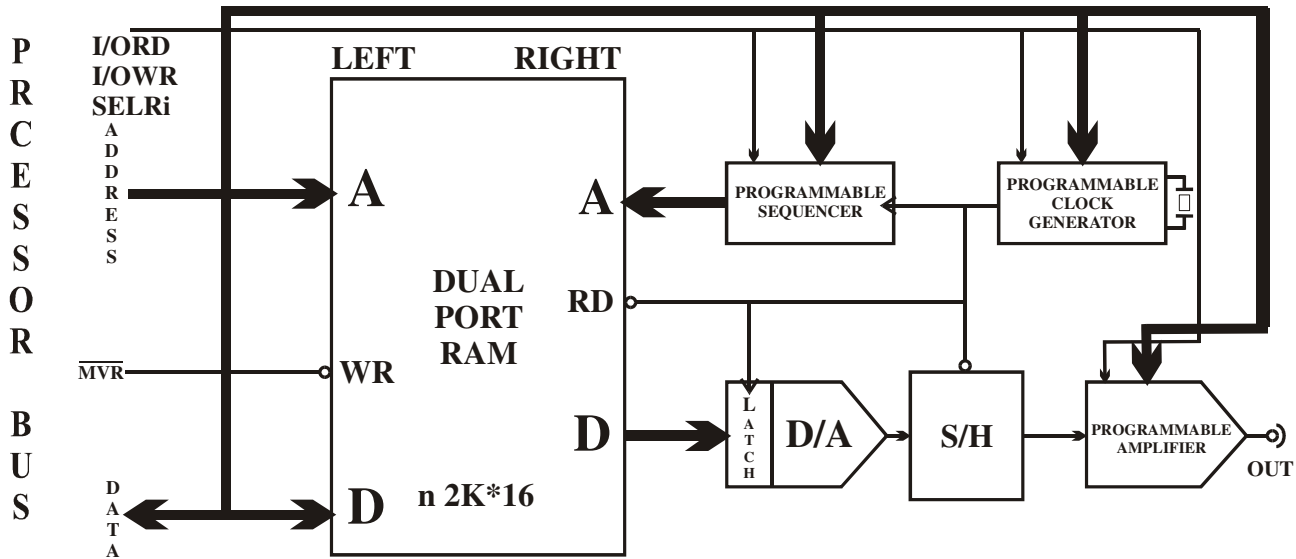


Fig. 1: Hardware Architecture of Arbitrary Waveform Synthesizer Modul

### 3. CONCLUSION

The suggested solution can find wide application in complex DPS systems and can satisfy the needs considering both the arbitrariness of wave forms and the accuracy ranging from the lowest frequencies up to ten megahertz. The hardware structure is based on standard elements – cells available for integrated circuits design.

### 4. REFERENCES

[1] Hasun R., and Kovalick A., "An Arbitrary Waveform Synthesizer for to 50 MHz", Hewlet Packard Journal, No. 3, April 1988.

[2] Jevtić M., Radenković V., Živanović D., and Vukčević B., "PC Module Arbitrary Waveform Synthesizer for to 25 MHz", Facta Universitatis, Series Electricis and Energetics, No. 1, Niš 1991.

[3] Radenković V., Jevtić M., Živanović D., and Vukčević B., "PC Module for Generating Arbitrary Waveforms in Automatical Measurement System", Proc.of AUTOMATION '92, pp 80 – 89, Budapest, 1992.

[4] SINE, COSINE on the TMS320C2xx, Application Report, Texas Instruments, BPRA047, November 1996.

## EXTENSION OF THE INPUT VOLTAGE RANGE OF FLYBACK CONVERTER BY MEANS OF IGBT

Vladimir Rajović, Nenad Jovičić, Slavoljub Marjanović, Faculty of Electrical Engineering Belgrade

**Abstract:** A coupling stage for extension of the input voltage range of flyback converter is described herein. A problem frequently faced in practice is described in brief; the coupling stage's electrical circuit and results of computer simulation are presented.

**Keywords:** Flyback converter, Insulated Gate Bipolar Transistor, overvoltage conditions.

### 1. INTRODUCTION

Flyback is the most commonly used low-power switching converter for getting low output voltage out of high input voltage. An example is getting 5V output DC voltage out of input mains voltage. The input voltage is being rectified first (full- or half- bridge) and coupled to an electrolytic capacitor and, finally, a flyback. There are two limitations with this:

- 1) The capacitor used should be able to handle rectified mains voltage, i.e. non-stabilized DC voltage.
- 2) The switching MOSFET within flyback should stand voltages much higher than the voltages applied to the electrolytic capacitor.

For an input mains voltage of 220V AC the capacitor should be able to stand a minimal voltage of 350V DC, whereas the MOSFET should have breakout voltage defined by the transformer's transformation ratio; this voltage is for sure higher than 350V. For certain industrial applications there is a need to secure the power supply to function properly in the case that instead of the line voltage (220V AC) the phase voltage (380V AC) is applied at the input. A regular flyback capable to stand such a change of input voltage should comprise oversized (in the sense of DC voltage) input electrolytic capacitor, nominated at 630V DC, and a MOSFET whose breakout voltage should be twice the case of line voltage at the input. Moreover, an additional

problem of the flyback control would occur, since a wide range of input voltage change would require a wide change of duty cycle; and it is a problem itself. All the abovementioned should cause a use of expensive components which function at boundaries of electrostatic endurance; this should then imply a lower device's reliability.

The solution presented in this paper consists of inserting a coupling stage between mains and the electrolytic capacitor at the input of the flyback; the stage controls charging of the capacitor. Therefore we could say that the stage is a controlled rectifier.

### 2. THE DESCRIPTION OF THE DEVICE

The electrical scheme of the device is shown in Figure 1. An Insulated Gate Bipolar Transistor (IGBT) is applied as the switching element. IGBT has good characteristics when one counts electrostatic endurance, as well as controlability. Comparing to three possible switching alternatives [1]:

- 1) IGBT is much more electrostatically robust and is having a higher transfer coefficient ( $B$ ) than MOSFET [2, 3]
- 2) IGBT needs no stimulating current, as opposite to bipolar transistors; it provides for a low-power control circuit.
- 3) IGBT is fully controllable, as opposite to thyristor.

IGBT is in the given configuration used as a unitalateral switch with resistance of magnitude order of  $0.1\Omega$  [4]. Control logic is founded on integrated CMOS timer circuit TLC555. The integrated circuit is not used in a timer configuration, but we use its internal composites – two comparators and SR latch. This provides for savings, since alternatively we should have to use at least two other integrated circuits (a dual comparator and a latch). Beside decreasing the needed area of a printed circuit board, and the

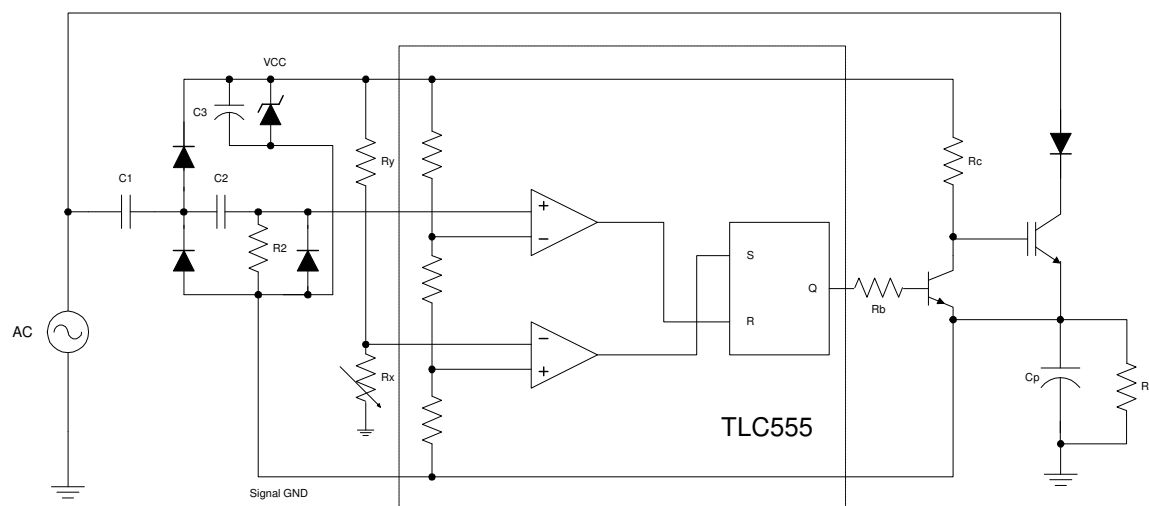


Figure 1. Electrical scheme of the device

fact that the integrated circuit TLC555 is very cheap (this could not be said for CMOS comparators) and widely available component, the advantage of this component is its power consumption, which is below 1mA at 10V [5]. Power supply of this component is secured by means of capacitive divider C1 – C3 and is equal to 10V. Because of such a low power consumption, the capacitors in the capacitive dividers could be smaller, C1 ~ 10nF, C3 ~ 10µF.

The great advantage of this device is that we avoid a use of high-side drivers for control of the switch, by the means of connecting signal ground to emitter of the IGBT. By this solution we gained possibility of direct control of the switch, from digital logic, and the need for coupling elements (optocouplers or high voltage low-power transistors) is eliminated.

The desired value of non-stabilized output voltage is adjusted by voltage divider Rx – Ry, according to the following equation:

$$R_x = \frac{R_y}{2} \left( 3 \frac{V_{out}}{V_{cc}} + 1 \right),$$

where  $V_{out}$  is the peak value of the non-stabilized voltage (in the moment of switching off the switch, i.e. turning off the IGBT), and  $V_{cc}$  is the supply voltage of the integrated circuit.

**3. THE PRINCIPLE OF THE DEVICE'S FUNCTION**

In the Figure 2. is shown the graph of input and output voltage and characteristic moments are marked; the graph is obtained by means of PSPICE simulation. At the output, a non-stabilized voltage of peak value of 300V is being maintained, whereas at the input is present phase voltage (380V AC). In the simulation we used the IGBT IRGBC20S [4].

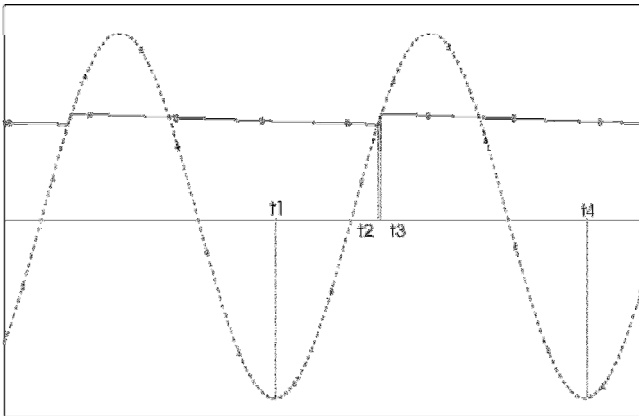


Figure 2. Input and output voltage in continuous regime

In the moment  $t_1$  input voltage falls down to its minimum and starts to rise. At the rise, regardless the momentary value of output voltage, the control logic is being supplied through the capacitive divider C1 – C3. In the same time the latch is being reset, through the same capacitive divider, differentiator C2 – R2, and comparator in the integrated circuit. It equalize the gate – emitter voltage to the logic's voltage supply (10V DC). When input voltage reaches the output voltage momentary value (the moment  $t_2$ ), the IGBT starts to conduct and act as a switch of magnitude order of 0.1Ω. From that moment on, the output voltage simultaneously changes with the input voltage.

The rise of the output voltage, through the resistive divider Rx – Ry, results with a relative fall of the voltage at the /trigger pin of TLC555 in relation to the signal ground. When the voltage falls down to 1/3 Vcc, thorough the second comparator the latch is being set, and the IGBT turns off. ( $t_3$ ).

The IGBT remains turned off until the input voltages falls down to its minimal value again (the moment  $t_4$ ).

The given simulation is done for a power supply of average 9W power. The dissipation of the series transistor is 65mW, whereas the total dissipation in the circuits amounts to 170mW. The coefficient of utilization equals to 98%.

The upper limit of the mains voltage which might be applied at the inout of the coupling stage is set only by breakout voltage of the collector – emitter junction. For the actual IGBT we used in the simulation, IRGBC20S, it equals to 420V AC.

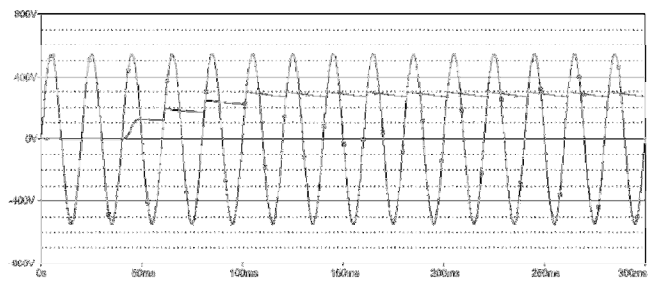


Figure 3. Input and output voltage in transient regime

The graph of input and output voltage in the course of 300ms after the device is powered-on, is given in Figure 3at je grafik ulaznog i izlaznog napona u toku prvih 300ms od uključenja uređaja. A continuous regime is reached after 100ms, when voltage supplu of control lofic become stable.

**4. CONCLUSION**

The solution described is elegant, since the device could be inserted, as an inter-stage, before any switching low-power power supply having a rectifier at its input. It has a high coefficient of utilization, consequently not depreciating the point of using switching power supply it is added to. It consists of a few cheap and widely available components. Consequently, it is of a small size. Reliability of the device is high, since the only component suffering voltage and current spikes, IGBT, is *per se* projected for such applications.

**5. REFERENCES**

- [1] N.Mohan, W.P.Robbins, T.M.Undeland, *Power Electronics*, Wiley
- [2] *IGBT Characteristics, AN-983, International Rectifier*
- [3] C.Blake, C.Bull, *IGBT or MOSFET: Choose Wisely, International Rectifier*
- [4] *IRGBC20S datasheet, International Rectifier*
- [5] *TLC555 datasheet, Texas Instruments*

## COMPARATIVE CHARACTERISTICS OF THICK FILM LC FILTERS WITH DIELECTRIC AND FERRITE LAYER

Vladan Desnica, Ljiljana Živanov, Fakultet tehničkih nauka Novi Sad, T.D. Obradovića 6  
Obrad Aleksic, Miloljub Luković, Elektrotehnički fakultet, Beograd, B.Revolucije 6  
Lazar Lukić, IRITEL A.D. Beograd, Batajnički put 23

**Abstract:** Attenuation and Smith charts of symmetrical LC filters were measured in range 1 MHz to 3 GHz. Three main LC filters were joined in series to sum attenuation. The obtained results were compared mutually, at first, and then with the optimized LC filters. We presented a analytical model and computer program for thick film integrated LC filters that is suitable for design, comparative and circuit simulation.

**Keywords:** Thick films, EMI filters, Symmetrical LC filters.

### 1. INTRODUCTION

During the last several years our research activities have been under way to develop and simulate integrated passive components that are part of the thick film circuit and are fabricated with the same production techniques as hybrid circuits [1]. This paper, based upon many experimental published works [2-12] where we have researched the planar inductive structures such as different kinds of spiral, meander and solenoid-bar type, gives a new concept for the EMI thick film passive component. Applications of thick film passive components are considered to be primarily in low cost, lightweight filter circuits and systems. The technique for development of thick film components is divided into three phases, as shown in Fig. 1. Development of thick film resistors, capacitors, inductors and varistors was done in the first phase, while R, L, C and V thick film components combinations was done in the second phase. In the third phase after the end of the second phase we start to development of LC and LCV filters and networks.

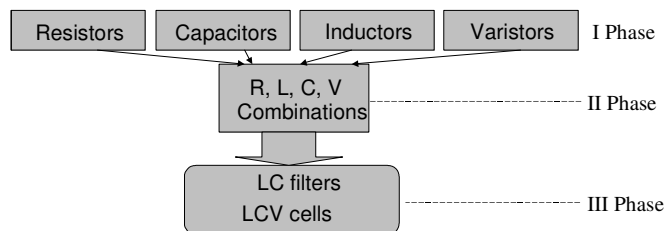


**Fig. 1. Block diagram for development of integrated passive components divided into phases.**

According to this experience, thick film symmetrical EMI LC filters were aimed to cover wide band of suppression with high attenuation in dB. They were designed as symmetrical and to act like EMI planar choke and planar capacitor between the main leads.

Using thick film technology 32 (thirty two) different LC filters with two pairs of terminations were realized for work in HF band.

Thick film LC filters were measured in range of 1MHz to 3 GHz on network analyzer HP 8752A, to obtain attenuation and Smith charts for complete characterisation. After that process modeling and simulation of LC filters were done. The obtained results were used for optimisation during filter design process, and for realisation of series combination

of two or three LC filters printed on alumina using dielectric and ferrite layer.

### 2. MODEL

Modeling of two-port LC filters ratiion between physical length of structure and wavelength. Filter dimensions, specifically the total coupled length are not always small compared to wavelength  $\lambda$  at operating frequency of interest. For speed of light ( $c=3 \times 10^8$  m/s), working frequency and wavelength  $\lambda$  of interest ( $\lambda=c/f$ ) are shown in Table 1.

$f = 100$ KHz	$\lambda = 3000$ m
$f = 1$ MHz	$\lambda = 300$ m
$f = 100$ MHz	$\lambda = 3$ m
$f = 1$ GHz	$\lambda = 0.3$ m = 30 cm
$f = 5$ GHz	$\lambda = 0.06$ m = 6 cm
$f = 10$ GHz	$\lambda = 0.03$ m = 3 cm

**Table 1. Working frequency versus wavelength, where  $f$  = frequency,  $\lambda$  = wavelength.**

Filter with  $\varphi$  (m), physical length could be represented by appropriate model:

- if  $\lambda_{\min} < \varphi$  with distributed circuit model, or
- if  $\lambda_{\min} < 4 \cdot \varphi$  with lumped equivalent model.

While characterising the symmetrical two-port integrated thick film LC filters we compute the capacitive and the inductive coupling separately, neglecting possible coupling between electric and magnetic fields. This approximation is acceptable as long as the physical length of the conductor is sufficiently small compared to the wavelength in the circuit. This approximation is valid for our distributed equivalent filter model if we use partial concept.

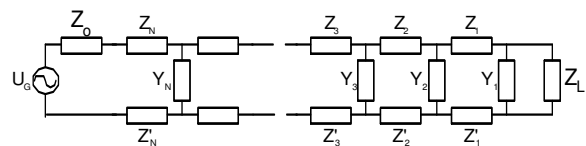


**Fig. 2. General distributed circuit model of LC filter.**

The distributed equivalent circuit model of symmetrical two-port integrated thick film filter, shown in Fig. 2, will characterise the component sufficiently enough, where all coupled segments of symmetrical two-port integrated thick film filter are represented with lumped elements, Fig. 3.

In the model, the main branches consist of: R - the series resistance caused by the finite conductivity of the metal, C - feedforward capacitance and L - the series inductance, while branch between coupled segments, represents the mutual coupling.

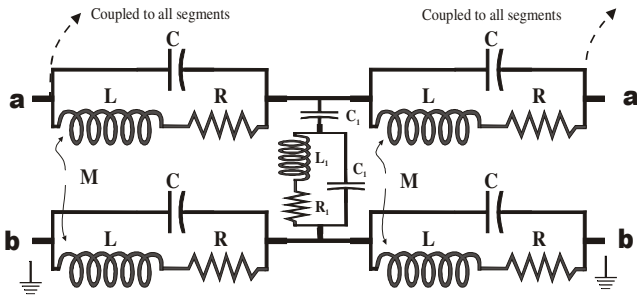


**Fig. 3. Lumped equivalent model of coupled segments.**

Modeling of symmetrical two-port integrated thick film filter resistance, inductance and capacitance is achieved utilizing equations from reference [2]. Attenuation,  $A_t$ , for distributed circuit model, from Fig. 2, is calculated by

$$A_t[dB] = 20 \log A_t = 20 \log \frac{Z(1) - Z_1 - Z'_1}{Z_0 + Z(N)} \cdot \prod_{i=1}^{N-1} \left( \frac{1}{1 + Y_{i+1} Z(i)} \right), \quad (1)$$

and

$$Z(i) = Y_i \parallel Z(i-1) + Z_i + Z'_i, \quad (i = 1, 2, \dots, N), \quad (i = 1, 2, \dots, N), \quad (2)$$

where  $N$  is number of sections,  $Z_i(Z'_i)$  is impedance per one block,  $Y_i$  is admittance per one block, and  $Z_L$  is load impedance.

Lumped-element and distributed circuit models are used for each optimised planar thick film filter [2-4]. In the case where the middle layer is ferrite material, filter model is little modified, because the permittivity and permeability of ferrite material are complex parameters consisting of real and imaginary part. The real component represents the reactive portion and the imaginary component represents the losses.  $R_f$  filter resistance in the ferrite environment is given by

$$R_f = 2 \cdot \pi \cdot f \cdot L_0 \cdot \mu''_r, \quad (3)$$

where  $f$  is frequency,  $L_0$  is inductance of inductor in vacuum environment and  $\mu''_r$  imaginary part of complex permeability. The impedance curve can be translated to a pure material curve, the so-called complex permeability curve. As impedance consists of reactive and resistive part, permeability should have two parts too to represent this. The real part corresponds to the reactance, positive for an inductance, negative for a capacitance, and the imaginary part to the losses. The impedance of the filter is given by

$$\begin{aligned} Z &= j\omega(\mu' - j\mu'') \cdot L_0 \\ &= \alpha\mu'' \cdot L_0 + j\alpha\mu' \cdot L_0, \end{aligned} \quad (4)$$

$$\begin{aligned} Z &= R + jX \rightarrow R = \alpha\mu'' \cdot L_0, \\ X &= \omega \cdot \mu' \cdot L_0 (\omega = 2 \cdot \pi \cdot f) \end{aligned} \quad (5)$$

$$|Z| = \sqrt{R^2 + X^2} = \omega \cdot L_0 \cdot \sqrt{\mu'^2 + \mu''^2}. \quad (6)$$

### 3. EXPERIMENTAL

Developed and measured symmetrical two-port LC filters were divided into three groups. Matrices, from the first group, were designed to cover the simplest geometries to complex geometries with two conductive layers that serve as the top and bottom of middle-cross-over layer, as shown in Fig. 4. Interaction between symmetrical two-port LC filters leads

was achieved using EM (electromagnetic) field (like choke windings) through dielectric layers. The best EMI (electromagnetic interference) noise suppression were obtained on filters number 5, 10, 13, 14 and 15 from the second group. While optimised LC filter structures from Fig. 5 represents the third group.

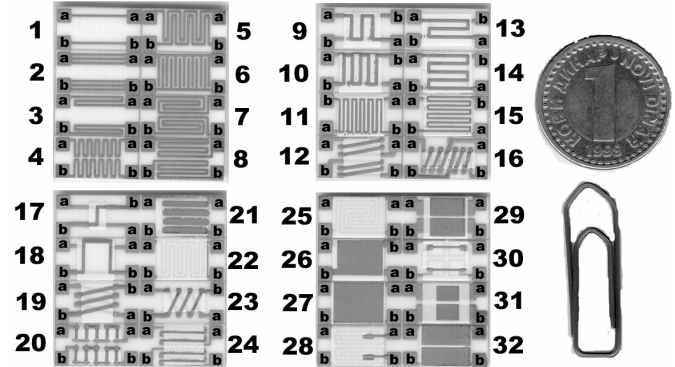


**Fig. 4. Top view of realized two-port LC filter matrices.**

The supreme attenuation on discrete frequencies for individual LC filter are collected in Table 2. Individual LC filters, as shown in Table 2, are similar to notch capacitive filters in the range of supreme attenuation.

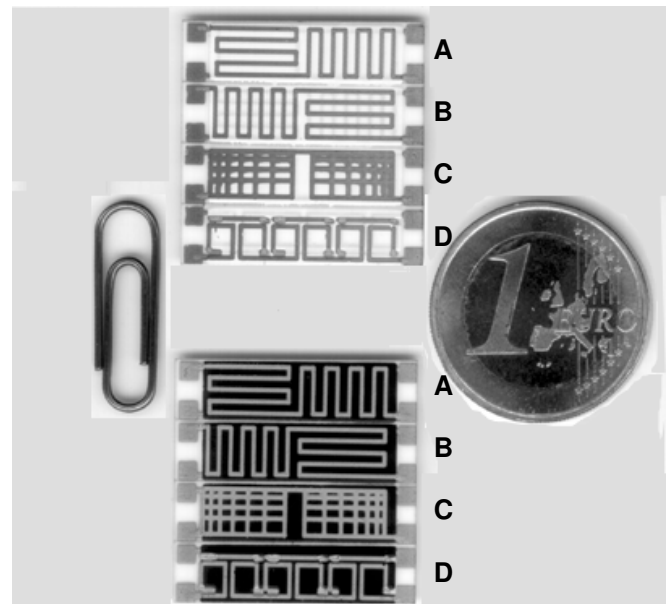


**Fig. 5. Top view of realized optimised two-port LC filter matrices. The paper clip and EURO indicate relative sizes.**

Aim to get wider suppression band a few series combinations were formed. Output terminations of one filter were joined to input terminations of another filter by soldering from edge to edge. Influence of parasitic inductance and capacitance of joints expected to be low enough. In order to isolate the influence of joint optimised thick film filters, from third group were realised.

FILTER.	Attenuation [dB]	f [MHz]	Attenuation [dB]	f [MHz]	Attenuation [dB]	f [MHz]
5	30	160	15	600	15	1800
7	15	2000				
10	50	50	30	300		
13	40	930				
14	30	600	25	1800		
15	50	1200	20	2700		
19	25	2000				
26	20	1600				
28	15	1600				
29	15	3000				
31	15	3000				

Table 2. Supreme attenuation summary for individual LC filters on discrete frequencies.

4. OPTIMISED DESIGN OF LC FILTERS.

Series combination of three LC filters was also formed to cover the widest EMI suppression range. Attenuation and Smith charts were plotted, for combination of filters such as 5+10+14, 10+13+14, 10+14+15 and 13+14+15. Measured results (M) obtained on network analyzer together with expected-simulated (summed) attenuation data (S) are given in Fig. 6-9.

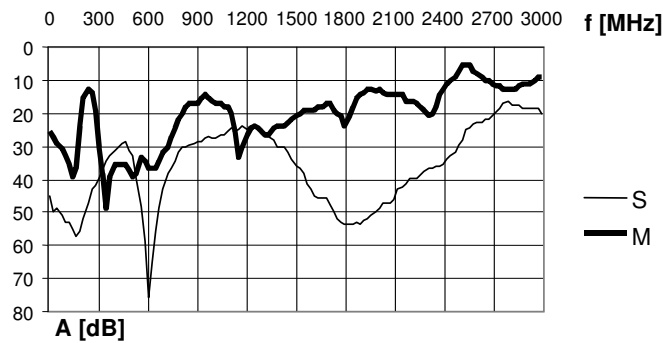


Fig. 6. Attenuation for series combination of LC filters 5, 10 and 14 (M-measured, S-simulated).

It has been shown that, in comparison with individual EMI LC filters, series combination of EMI LC filters yield higher attenuation as well as higher usable frequency range. These individual EMI LC filters have a high attenuation of less than 40 dB.

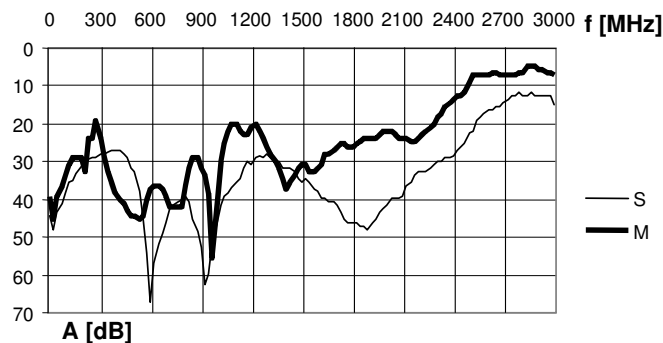


Fig. 7. Attenuation for series combination of LC filters 10, 13 and 14 (M-measured, S-simulated).

While combinations of two EMI LC filters give attenuation of 30 dB in frequency band of few hundred MHz, and attenuation of 20 dB in 2 GHz wide frequency band. Combinations of three EMI LC filters could give us 10 dB more attenuation in the much wider frequency ranges. Also, the usable frequency range of cubic SMT EMI filters is generally reduced as compared to series combination of EMI LC filters. The variation of attenuation and complex impedance of EMI LC filters can be tuned to desired value by geometrical adjustment of EMI LC filters parameters.

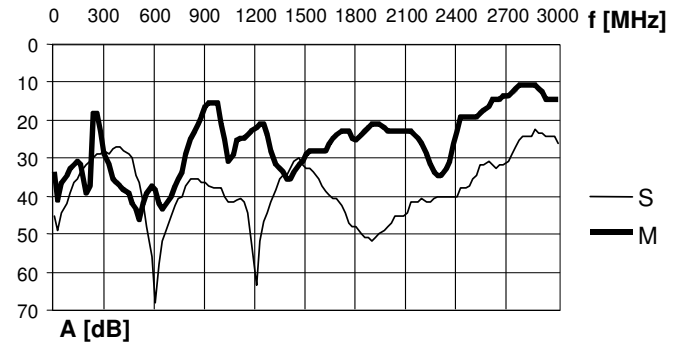


Fig. 8. Attenuation for series combination of LC filters 10, 14 and 15 (M-measured, S-simulated).

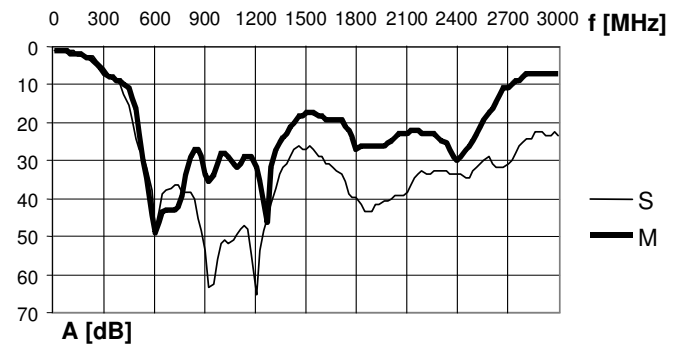


Fig. 9. Attenuation for series combination of LC filters 13, 14 and 15 (M-measured, S-simulated).

Table 3 shows how adding the additional EMI LC filters can increase the attenuation value in wider band.

Tri filtra	5+10+14	13+14+10	14+10+15
Realni [Ω]	50,416	51,865	52,301
Imaginarni [Ω]	0,7207	1,4707	0,5957
Impedansa [Ω]	50,42	51,88	52,3
f [MHz]	150	100	100
Realni [Ω]	51,459	50,08	50,311
Imaginarni [Ω]	-548,83m	0,5	0,373
Impedansa [Ω]	51,46	50,08	50,31
f [MHz]	473	500	500
Realni [Ω]	61,307	48,811	53,414
Imaginarni [Ω]	-11,551	0,6035	-5,7832
Impedansa [Ω]	62,38	48,81	53,73
f [MHz]	1000	1000	1000
Realni [Ω]	49,104	56,439	54,713
Imaginarni [Ω]	-22,457	-4,6289	-6,2734
Impedansa [Ω]	53,99	56,62	55,07
f [MHz]	2000	2000	2000

Table 3. Complex impedance summary for series combination of three LC filters.

Fig. 9 shows the simulated and measured values of attenuation for optimised planar thick film filter B. We compared the influence of dielectric middle layer for dielectric constants of interest. The equivalent circuit analysis shows the contribution of the magnetic film to the optimised planar thick film filter. By applying the magnetic film to the optimised planar thick film filter. By applying the magnetic film to the dielectric middlelayer filter attenuation was increased from 1 to 3 GHz.

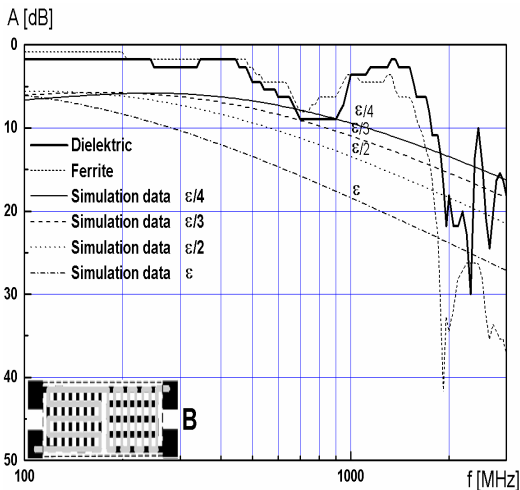


Fig. 10. Measured and simulated attenuation for optimised planar thick film filter B.

## 5 CONCLUSION

Four matrices, with 32 different LC filter designs, were described and experimental filters were fabricated using a standard thick film system. Thick film symmetrical EMI LC filters are new class of planar EMI filters with two pairs of terminations. They are symmetrical from input to output and from one lead to another in the pair. This type of EMI filter is similar to LCV cells [15], which have three terminations (input, output and ground), but they act otherwise.

The distributed equivalent circuit model of EMI LC filter, shown in Fig. 2, will characterize the component sufficiently enough, where all coupled segments of EMI LC filters are represented with lumped elements, Fig. 3. The effects of EMI LC filters could be best explained by taking into account frequency characteristics of alumina and crossover, dielectric permittivity,  $\epsilon_r(\omega)$ . The measuring of dielectric characteristics allows better calculating of data relative to material of the structure in order to isolate the design parameter of the intrinsic EMI LC filter.

## ACKNOWLEDGEMENT

The authors of this paper have, along with a number of Serbian partners, spent the last few years working on a Serbian Ministry of Science, Technology and Development funded project, 10E05, and ETR.6.04.32023B. The authors highly appreciate the important support of the Republic of Serbia.

## 6. REFERENCES

- [1] V. Desnica, Lj. Živanov, O. Aleksić, S. Jenei, "Modeling and optimization of thick film solenoid-bar type inductors and transformers", *COMPEL (Computation and Mathematics in E.E.E.)*, Vol. 19, no. 2, pp. 615-621, 2000.
- [2] V. Desnica, Lj. Živanov, M. Nimrihter, O. Aleksić, M. Luković, "A Comparative Characteristics of Thick Film Integrated LC Filters", *IEEE Transactions on Instrumentation and Measurement*, vol. 51, no. 4, pp.570-576, August 2002.
- [3] Desnica, V., Živanov, Lj., Aleksić, O. (2000) "Thick Film Integrated LC Cells", 4th Symposium Of Electronics And Telec. ETC'2000, Timisoara, RO, Vol.2, pp.42-5.
- [4] O. Aleksić, L. Lukić, "Analiza svojstva Ni-Zn ferita u EMI opsegu", *NTB 1-2*, pp. 11-18, 2000.
- [5] O. Aleksić, M. Luković, J. Ristović, "EMI zaštita u SMT modulima", *NTB 1*, pp. 61-72, 2001.
- [6] Desnica, V., Živanov, Lj., Nimrihter, M., Aleksić, O., Luković, M. (2001) "A Comparative Characteristics of Thick Film Integrated LC Filters", 18th IEEE Instrument. and Measurement Technology Conf., Budapest, Hungary, vol. 2, pp. 1016-20.
- [7] Desnica, V., Živanov, Lj., Aleksić, O. (2001), "The modeling and design of symmetrical thick film EMI/EMC cells", *ISEF/2001-10th International Symp. on Electr. Fields in Electrical Eng.*, Cracow, Poland, pp. 257-62.
- [8] Desnica, V., Živanov, Lj., Aleksić, O. (2001) "Thick Film EMI/EMC Filters", 11th International Symposium on Power Electronics Ee2001, Novi Sad, YU, pp.139-42.
- [9] Desnica, V., Živanov, Lj., Aleksić, O. (2002), "Symmetrical thick film EMI/RFI filters", 23rd International Conference on Microelectronics MIEL 2002, Niš, Yugoslavia, vol. 1, pp. 361-364.
- [10] V. Desnica, Lj. Živanov, O. Aleksić, M. Luković, L. Lukić, "Symmetrical Two-port Integrated Thick Film Filters", *Interconnection and Packaging Symposium IMAPS 2002 Proceedings*, pp. 312-316, Cracow, Poland.
- [11] O. Aleksić, V. Desnica, M. Luković Lj. Živanov, "Thick film symmetrical EMI LC cells", *Microelectronics International*, vol. 19, no. 2, pp. 19-25, 2002.
- [12] V. Desnica, Lj. Živanov, O. Aleksić, "The modeling and design of symmetrical thick film EMI/EMC cells", *Studies in Applied Electromagnetics and Mechanics: Electromagnetic Fields in Electrical Engineering*, vol. 22, pp. 395-400, IOS Press, Amsterdam, 2002.
- [13] L. Martens, "High-Frequency Characterization Of Electronic Packaging", Kluwer Academic Publishers, Boston/Dordrecht/London, 1998.
- [14] M. Mardigniar, "EMI Troubleshooting Techniques", McGraw-Hill, SAD, 2000.
- [15] O. Aleksić, P. Nikolić, M. Luković, D. Vasiljević-Radović, "Planar thick film integrated LCV cells", *Microelectronics International*, Vol. 38, pp 12-15, 1995.

# IMPROVED METHOD FOR OPTIMISATION OF INDUCTORS USING GEOMETRIC PROGRAMMING

Goran Stojanovic, Ljiljana Zivanov, Mirjana Damnjanovic, Faculty of Technical Sciences, Novi Sad

**Abstract:** In this paper, we present an approach to improve the optimisation of spiral inductors fabricated in a semiconductor process by use of geometric programming (GP). For optimisation of spiral inductors, the GP-based tools offer significant advantages over the other techniques. The primary advantages are reduced optimisation time and computer resources. Also, the designer has more flexibility to try variations of the spiral layouts or optimise them for a desired behavior.

**Keywords:** spiral inductor, geometric programming, optimisation, quality factor.

## 1. INTRODUCTION

The computer tool for optimization inductor by use of geometric programming technique has been already used for finding optimal design for topology of an LC oscillator [1],[2]. In this paper will be presented efficient and fast method for finding optimal design of a spiral inductor in conformity to a new approach in defining of objective function. Different geometric programming algorithm is proposed, with different objective function, with less number of constraints, faster method than the one in proposed literature [2]. The software tool for optimization of inductor, is "user friendly", very intuitive and simple for use and it is just one part of the computer tool for drawing layout and simulation of monolithic spiral inductors.

## 2. GEOMETRIC PROGRAMMING

GP is one of the more recent developments in optimization theory. GP is a particularly powerful method for engineering design and optimization problems. GP was first introduced by *Duffin, Peterson* and *Zener* [3] in their seminal book, and another important source of information is the book by *Beightler* and *Phillips* [4], in involved algorithm by *Blau* which is basis our implemented algorithm. Engineering design is most natural application for GP since in most design problems, the total cost can be expressed as the sum of individual component costs, each of which is in generally some power function of design variables. This is the format required by GP; the individual components of additive polynomial cost function are expressed as the product of a cost coefficient and individual design variables, each raised to some constant power.

A geometric programming problem having  $N$  variables and  $M$  constraints can be represented as:

Minimize:

$$y_o(x) = \sum_{t=1}^{T_0} \sigma_{ot} \cdot c_{ot} \prod_{n=1}^N x_n^{a_{otn}} \quad (1)$$

Subject to constraints of geometric form:

$$\sum_{t=1}^{T_m} \sigma_{mt} \cdot c_{mt} \prod_{n=1}^N x_n^{a_{mnt}} \leq \sigma_m, \text{ za } m=1, 2, \dots, M \quad (2)$$

$\sigma_{ot}$  and  $\sigma_{mt} = \pm 1$  (the sign of each term in the objective function and  $m^{\text{th}}$  constraint, respectively),  $c_{ot}$  and  $c_{mt} > 0$  (the coefficients of each term in the objective function and  $m^{\text{th}}$  constraint, respectively),  $x_n > 0$  (the independent variables),  $\sigma_m = \pm 1$  (the constant bound of the  $m^{\text{th}}$  constraint),  $a_{otn}$  and  $a_{mnt}$  (are the exponents of the  $n^{\text{th}}$  independent variable of the  $t^{\text{th}}$  term of objective function and  $m^{\text{th}}$  constraint, respectively),  $M$  (is the number of constraints),  $N$  (is the number of variables),  $T_0$  (is the number of terms in the objective function),  $T_1, T_2, \dots, T_M$  (are the number of terms in each constraint, 1 to  $M$ , respectively),  $\sigma = \pm 1$  (assumed sign of the objective function).

When  $T_0 = 1$  objective function is called a monomial function, while the sign of each term in the objective function or the constraint functions determines whether the polynomials is a posynomial (if  $\sigma_{ot}$  or  $\sigma_{mt} = +1$ ) or a signomial (if  $\sigma_{ot}$  or  $\sigma_{mt} = -1$ ).

Geometric programming method is global, meaning that it finds the absolute best design possible, when specification are feasible. The starting point for GP does not have any effect on the optimal solution, and user no set starting point values.

## 3. PLANAR SPIRAL INDUCTORS

### 3.1 Variables for optimization

In the figure 1 is shown the layout of a square planar inductor. The variables for optimisation that characterize the inductor geometry are: the number of turns -  $n$ , the width of conductor segment -  $w$ , the spacing between naiberhoid conductor segment -  $s$ , the outer diameter -  $d_{out}$  and the average diameter -  $d_{avg}$ , which can be expressed as  $d_{avg} = 0.5(d_{out} + d_{in})$ . These five variables are not independent, but in the open literature it will be convenient to consider this set of variables.

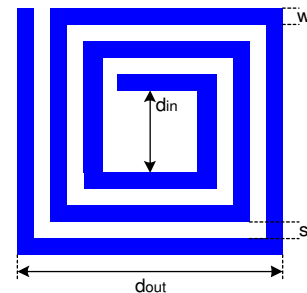


Fig. 1. Layout of planar spiral inductor.

We also note that the design variables are discrete ( $w, s, d_{out}$ ), while the number of turns  $n$  is restricted to take values that are integer multiples of 0.25 (quarter turns). However, we ignore these grid constraints and consider the variables to be continuous. In every design we have carried out, this step has caused no significant error. Another geometry parameters such as the total length of inductor or the inductor area is very significant that to be defined. Thus,

the total length of inductor can be expressed as  $l=4 \cdot n \cdot d_{avg}$ , and the inductor area  $A=d_{out}^2$ .

### 3.2. Electrical model of inductor

All the results in this paper are based on a relatively simple, reasonably accurate one-port model for inductors shown in Figure 2 (a) and simplified model shown in Figure 2 (b) [5]. In this section, we present expressions for model parameters in the geometric programming form. Each parameter is a monomial or posynomial function of the design variables and a coefficient that is dependent on technology and frequency.

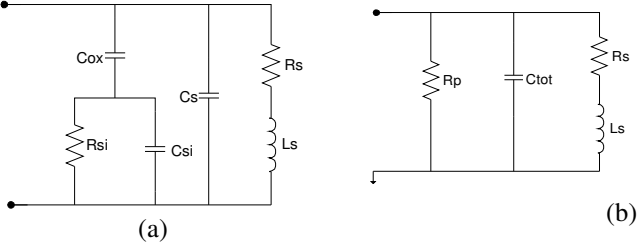


Fig. 2. (a) One-port model of planar spiral inductor (b) simplified model of planar spiral inductor.

**Inductance Ls.** The formula from [6]

$$L_S = \beta \cdot d_{out}^{\alpha_1} \cdot w^{\alpha_2} \cdot d_{avg}^{\alpha_3} \cdot n^{\alpha_4} \cdot s^{\alpha_5}, \quad (3)$$

is a monomial expression, obtained by fitting technique, with six fitting factors and with inductance in nH and dimensions in  $\mu\text{m}$ . The coefficients  $\beta$  and  $\alpha_i$  are only layout dependent and do not depend on the technology. For square spiral inductor values fitting factors are  $\beta = 1.66 \cdot 10^{-3}$ ,  $\alpha_1 = -1.33$ ,  $\alpha_2 = -0.125$ ,  $\alpha_3 = 2.5$ ,  $\alpha_4 = 1.83$ ,  $\alpha_5 = -0.022$  [6]. Because to simplicity notation and close to mathematical notation we introduced next equality:  $d_{out} = \mathbf{x}_1$ ,  $w = \mathbf{x}_2$ ,  $d_{avg} = \mathbf{x}_3$ ,  $n = \mathbf{x}_4$ ,  $s = \mathbf{x}_5$ . In accordance with these the formula (3) can be expressed as

$$L_S = 1.66 \cdot 10^{-3} \cdot x_1^{-1.33} \cdot x_2^{-0.125} \cdot x_3^{2.5} \cdot x_4^{1.83} \cdot x_5^{-0.022} \quad (4)$$

For this values of coefficients expression (4) is an accurate (typical error is to 3%) fit of the inductance in very broad design space.

**Resistance Rs.** The series resistance is given by the monomial expression (5)

$$R_S = \frac{l}{\left( \sigma \cdot w \cdot \delta \cdot \left( 1 - e^{-\frac{l}{\delta}} \right) \right)} = \frac{k_1 \cdot l}{w}, \quad (5)$$

where  $\sigma$  is the conductivity,  $t$  is the thickness of conductor segments, and  $\delta$  is the skin depth  $\delta = \sqrt{2 / (\omega \cdot \mu_0 \cdot \sigma)}$ , where  $\omega = 2 \cdot \pi \cdot f$ , and  $f$  is frequency and  $\mu_0 = 4 \cdot \pi \cdot 10^{-7}$  H/m is the magnetic permeability of free space. After substitution expression for  $l$  and introduce notation with  $x$  is given

$$R_S = K_1 \cdot x_2^{-1} \cdot x_3 \cdot x_4. \quad (6)$$

For example, for inductor with thickness of aluminum conductor segments  $0.9 \mu\text{m}$  and for frequency 2.5GHz gives  $K_1 = 0.171$ .

**Oxide capacitance Cox.** Oxide capacitance between the spiral and substrate can be approximated by the monomial expression

$$C_{ox} = \frac{\epsilon_{ox} \cdot l \cdot w}{2 \cdot t_{ox}} = k_2 \cdot l \cdot w, \quad (7)$$

where  $\epsilon_{ox}$  is the oxide permittivity, and  $t_{ox}$  is the oxide thickness. After simple mathematical operation expression (7) becomes

$$C_{ox} = K_2 \cdot x_2 \cdot x_3 \cdot x_4. \quad (8)$$

**Series capacitance Cs.** This capacitance can be modeled by the monomial expression

$$C_S = \frac{\epsilon_{ox} \cdot n \cdot w^2}{t_{ox, M1-M2}} = k_3 \cdot n \cdot w^2, \quad (9)$$

where  $t_{ox, M1-M2}$  is the oxide thickness between the spiral and the metal under-pass (for contact). Formula (9) can be expressed, also, such

$$C_S = K_3 \cdot x_2^2 \cdot x_4. \quad (10)$$

**Substrate capacitance Csi.** The silicon substrate capacitance is given by the monomial expression

$$C_{si} = \frac{C_{sub} \cdot l \cdot w}{2} = k_4 \cdot l \cdot w, \quad (11)$$

where  $C_{sub}$  is substrate capacitance per unit area and is dependent on permittivity of substrate and thickness of substrate. After simple modification formula (11) can be expressed such

$$C_{Si} = K_4 \cdot x_2 \cdot x_3 \cdot x_4. \quad (12)$$

**Substrate resistance Rsi.** The substrate resistance can be expressed as the monomial

$$R_{Si} = \frac{2}{G_{sub} \cdot l \cdot w} = \frac{k_5}{l \cdot w}, \quad (13)$$

where  $G_{sub}$  is the substrate conductance per unit area and is dependent on resistivity of substrate and thickness of substrate. The expression (13) can be given such

$$R_{Si} = K_5 \cdot x_2^{-1} \cdot x_3^{-1} \cdot x_4^{-1}. \quad (14)$$

The simplified model of planar spiral inductor is shown in Figure 2 (b). The total parallel capacitance,  $C_{tot} = C_s + C_p$ , is posynomial, and parallel resistance  $R_p$  is monomial. The parameters  $R_p$  and  $C_{tot}$  are frequency dependent and can be given such as follow:

**Parallel resistance Rp.** This resistance is given by the monomial expression

$$R_p = \frac{1 + [w \cdot R_{Si} \cdot (C_{Si} + C_{ox})]^2}{w^2 \cdot R_{Si} \cdot C_{ox}^2} = \frac{k_6}{l \cdot w}. \quad (15)$$

or in other mathematical notation

$$R_p = K_6 \cdot x_2^{-1} \cdot x_3^{-1} \cdot x_4^{-1}. \quad (16)$$

**Parallel capacitance Cp.** The parallel capacitance is given by the following expression

$$C_p = \frac{C_{ox} + w^2 \cdot R_{Si} \cdot (C_{Si} + C_{ox}) \cdot C_{Si} \cdot C_{ox}}{1 + [w \cdot R_{Si} \cdot (C_{Si} + C_{ox})]^2} = \quad (17)$$

$$= k_7 \cdot l \cdot w + k_8 \cdot (l \cdot w)^2$$

other words

$$C_p = K_7 \cdot x_2 \cdot x_3 \cdot x_4 + K_8 \cdot x_2^2 \cdot x_3^2 \cdot x_4^2. \quad (18)$$

We note, again, that coefficients  $K_i$ , (for  $i=1,2,\dots,8$ ) are dependent on technology and frequency.

#### 4. CONSTRAINTS AND IMPROVEMENT FOR OPTIMAL DESIGN OF INDUCTORS

A geometric program requires each of the constraint functions (or our objective function) to be a monomial, posynomial or a signomial for a difference to [1], [2] which is restricted to be either monomial or posynomial. Each constraints function can be less then or equal to 1 or equal to 1.

**Constraints for  $L_s$ .** Expression for inductance in geometric programming form is given by (4) and our software tool require the inductance to equal some specific value

$$L_s = L_{zelj}. \quad (19)$$

We can also impose a similar constraint for the serial resistance  $R_s$  or the total capacitance  $C_{tot}$ , for example.

**Geometry constraints.** Since, width of conductor segment ( $w$  in reference to  $x_2$ ) and spacing between conductor segment ( $s$  in reference to  $x_5$ ) to belong to optimization variables, very simple, it can be constrained. For example,

$$w \geq w_{\min} \text{ ili } s \geq s_{\min}. \quad (20)$$

We note that five variables are not independent. The average radius  $d_{avg}$  is related to the other design variables by the following expression:

$$d_{avg} = d_{out} - (n-1) \cdot s - n \cdot w. \quad (21)$$

**Quality factor.** The quality factor of an inductor, via parameters of the one-port model shown in the Figure 2 (b), can be defined as follows

$$Q_L = \frac{\omega \cdot L_s}{R_s} \cdot \frac{R_p \left( 1 - \frac{R_s^2 \cdot C_{tot}}{L_s} - \omega^2 \cdot L_s \cdot C_{tot} \right)}{R_p + \left[ \left( \frac{\omega \cdot L_s}{R_s} \right)^2 + 1 \right] \cdot R_s}. \quad (22)$$

However, the problem is because equation (22) is not written in geometric programming form. In references [2], this problem is solved thus is introduced one new variables  $Q_{L\min}$  or  $x_6$  and in the objective function this variables is maximize. An additive constraints can be written as  $Q_L \geq Q_{L\min}$ . This approach is correct, but introduced one variables more and one new constraints more. For difference to this, in our software tool we suggest the next approach.

Let us find the best possible expression for Q-factor, thus it can be written in geometric programming form (an signomial expression), near a true quality factor (7) in all frequency range. This approach is enabled type of our implemented algorithm in which objective function and constraints functions can be written in monomial, posynomial and signomial form (for difference to program in [2]). This difference is crucial in the context to reduce the CPU time for optimization. We found the next expression for the Q-factor in the geometric programming form

$$Q_L = \frac{\omega \cdot L_s}{R_s} - \omega \cdot R_s \cdot C_{tot} - \frac{\omega^3 \cdot L_s^2 \cdot C_{tot}}{R_s}. \quad (23)$$

After simulation we are concluded that difference of expression (22) and (23) is less then 0.1 % in all frequency range of interest (from 100MHz to 7GHz) and for different values inductance. As illustration, after simple mathematical operation, expression for Q-factor in the geometric programming form is as follows (for inductance 12nH)

$$Q_L = 1100.256 \cdot x_2 \cdot x_3^{-1} \cdot x_4^{-1} - 35639 \cdot 10^{-12} \cdot x_3^2 \cdot x_4^2 - 73.79 \cdot 10^{-18} \cdot x_2 \cdot x_3^3 \cdot x_4^3 - 92630 \cdot 10^{-12} \cdot x_2 \cdot x_3 \cdot x_4^2 - 43.26 \cdot 10^{-3} \cdot x_2^2 - 89.55 \cdot 10^{-12} \cdot x_2^3 \cdot x_3 \cdot x_4 - 112.46 \cdot 10^{-15} \cdot x_2^3 \cdot x_3, \quad (24)$$

where, again values  $x_1=d_{out}$ ,  $x_2=w$ ,  $x_3=d_{avg}$ ,  $x_5=s$  are in  $\mu\text{m}$ . In optimization process this objective function (24) is maximized in accordance with specifications for constraints. Thus, another specific value for inductance give different coefficients of each term, but function form and the exponents of the independent variable are stay the same.

**Constraint for minimum self-resonance frequency.** The self-resonance frequency  $\omega_{sr}$  is the frequency at which the quality factor, expression (22), equal 0. We want that the self-resonance frequency is greater then or equal to exactly specific value (minimum self-resonance frequency), that means  $\omega_{sr} \geq \omega_{sr, \min}$ . This condition can be written as follows

$$\omega_{sr, \min}^2 \cdot L_s \cdot C_{tot} + \frac{R_s^2 \cdot C_{tot}}{L_s} \leq 1. \quad (25)$$

In the geometric programming form, expression (25) for specific value for inductance 12nH is given

$$307.83 \cdot 10^{-6} \cdot x_2 \cdot x_3 \cdot x_4 + 637.23 \cdot 10^{-15} \cdot x_2^2 \cdot x_3^2 \cdot x_4^2 + 800.25 \cdot 10^{-6} \cdot x_2^2 \cdot x_4 + 32.33 \cdot 10^{-12} \cdot x_2^{-1} \cdot x_3^3 \cdot x_4^3 + 66.83 \cdot 10^{-21} \cdot x_3^4 \cdot x_4^4 + 83.33 \cdot 10^{-12} \cdot x_3^3 \cdot x_4^3 \leq 1. \quad (26)$$

#### 5. RESULTS FOR OPTIMAL DESIGN OF INDUCTORS

One much used figure of merit for the inductor characterization is the quality factor (Q-factor), which we have already introduced in the previous chapter. The Q-factor of an inductor is a figure of merit of usefulness of the component. With practical aspect we want to maximize Q-factor for a specific value inductance and for a minimum self-resonance frequency. In order to demonstrate our optimisation program we represented geometric programming problem as

$$\begin{aligned} & \text{maximize} && Q_L \\ & \text{subject to} && \end{aligned} \quad (27)$$

$$L = L_{zelj}, s \geq s_{\min}, \omega_{sr} \geq \omega_{sr, \min}, \quad (28)$$

In the figure 3 is shown maximum Q-factor at 2.5GHz versus inductance value for the same test inductor as in [2] (with PGS). Constraints are  $s \geq 1.9\mu\text{m}$  for a curve 1, and for curve 2 is added constraint for minimum self-resonance frequency as  $\omega_{sr} \geq 7\text{GHz}$ .

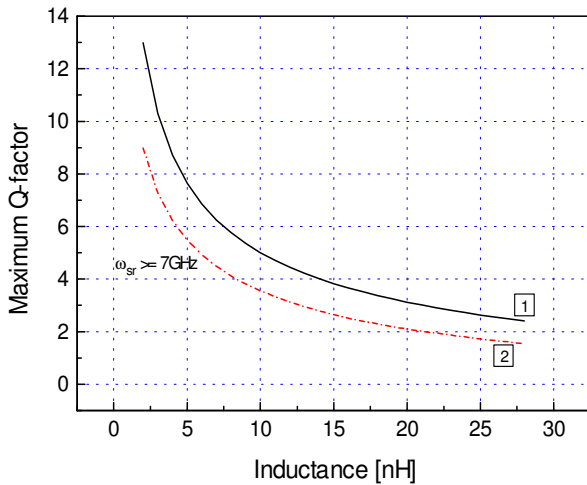


Fig. 3. Maximum  $Q$ -factor of inductor versus inductance

Note that when  $\omega_{sr}$  is not constrained one obtains a higher maximum quality factor. The results our program presented in the figure 3 and Table 1 show excellent agreement when compared with the measured data in open literature [2]. Our program gives graphical view for trade-off curves in an approximately one second (important advantage in compare with another programs in references)

In the figure 4 is shown optimal curve dependence  $Q$ -factor of spiral inductor for different value inductance. The simulation are performed for the space between conductor segment  $s \geq 25\mu\text{m}$  for curve 1, and for curve 2 is added constraint for minimum self-resonance frequency as  $\omega_{sr} \geq 5\text{GHz}$  and for curve 3 is added constraint for minimum self-resonance frequency as  $\omega_{sr} \geq 8\text{GHz}$ . The greater value of the space between conductor segment  $s$  gives smaller value of  $Q$ -factor.

## 6. CONCLUSIONS

In this paper, a efficient optimisation algorithms via geometric programming has been proposed. We are presented how elements of model spiral inductor can be written in the posynomial form, and how objective function can be written in the signomial, monomial or posynomial form. Our developed software tool can radically reduce optimisation times for optimal design planar spiral inductor, while still keeping the desired accuracy. After a successful optimisation it is possible quickly to draw the global trade-off curves maximum  $Q$ -factor versus inductance.

## 7. ACKNOWLEDGMENT

This work is partially funded by Project IT.1.04.0062.B.

## 8. REFERENCES

[1] Sunderarajan S. Mohan, Maria del Mar Hershenson, Stephen P. Boyd, and Thomas H. Lee: "Bandwidth extension in CMOS with optimized on-chip inductors", *IEEE Jour. of Solid-State Circuits*, vol. 35, no. 3, march 2000, pp. 346-355.

Table 1. Maximum  $Q$ -factor and optimal value of geometry parameters for some inductance value.

Inductance [nH]	Maximum $Q$ -factor					
	$d_{out}$ [ $\mu\text{m}$ ]	$w$ [ $\mu\text{m}$ ]	$d_{avg}$ [ $\mu\text{m}$ ]	$n$	$s$ [ $\mu\text{m}$ ]	
without constrained $\omega_{sr}$						
6	6.86					
	324.5;	18.7;	245;	3.9;	1.9	
12	4.45					
	246.9;	7.7;	186.9;	6.4;	1.9	
18	3.37					
	217.1;	4.6;	144.3;	8.4;	1.9	
24	2.72					
	201.9;	3.2;	152.9;	10;	1.9	
with constrained $\omega_{sr}$ ( $\omega_{sr} \geq 7\text{GHz}$ )						
6	4.92					
	198.4;	7.6;	153.7;	4.9;	1.9	
12	3.12					
	160.9;	3.1;	123.6;	7.8;	1.9	
18	2.29					
	148.6;	1.8;	113.7;	9.9;	1.9	
24	1.79					
	143.9;	1.2;	109.2;	11.5;	1.9	

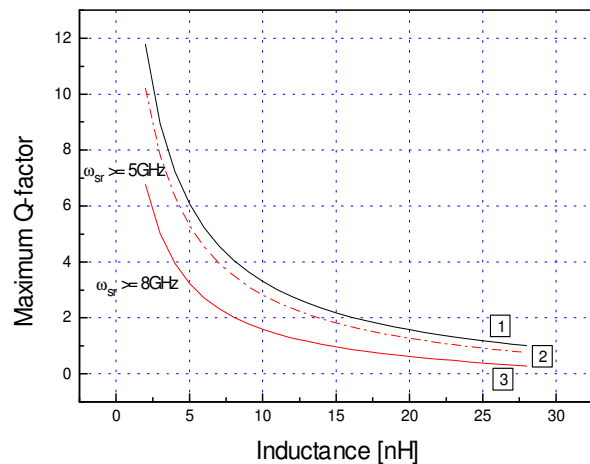


Fig. 4. Maximum  $Q$ -factor of inductor versus inductance

[2] M. Hershenson, S. S. Mohan, S. P. Boyd, and T. H. Lee: "Optimization of inductor circuits via geometric programming", in *Proc. Design Automation Conf.*, session 54.3, June 1999, pp. 994-998.

[3] R. J. Duffin, E. L. Peterson, and C. Zener: "Geometric programming – theory and applications", Wiley, 1967.

[4] Charles S. Baighler and Donald T. Phillips: "Applied geometric programming", New York, Wiley, 1976.

[5] C. Patrick Yue, C. Ryu, J. Lau, T. H. Lee, S. S. Wong: "A physical model for planar spiral inductors on silicon", *Proc. of IEDM'96*, 1996, pp. 155-158.

[6] Sunderarajan S. Mohan, Maria del Mar Hershenson, Stephen P. Boyd, and Thomas H. Lee: "Simple accurate expressions for planar spiral inductances", *IEEE Journal of Solid-State Circuits*, vol. 34, no. 10, october 1999, pp. 1419-1424.

## STRUCTURE, TECHNOLOGIES AND COMPONENTS OF DWDM SYSTEMS

*Ivanković Snežana, Faculty of Electrical Engineering in Belgrade*

**Abstract:** In this paper is discussed about fundamentals of DWDM (Dense Wavelength Division Multiplexing) systems. In the first part, structure is explained and in the second part technologies, like multiplexing and demultiplexing. The third part is about components in DWDM systems (optical fibers, sources, amplifiers, detectors and commutators).

**Keywords:** amplifiers, wavelength multiplexing, demultiplexing, optical fibers, channel spacing, switchers

### 1. INTRODUCTION

Because of growing of demands in the field of communications, the need for optical fibers rises. Most advantage of the DWDM technologies considering the technical and economical aspect is the potentially limitless transfer capacity, which can be achieved by either using improved equipment or by increasing number of wavelength in the fiber without expensive system upgrading. Further advantages of DWDM systems are also transparency, scalability and dynamical provision. (supply).

### 2. EVOLUTION

The evolution of optic fibers is closely connected to the part of optical spectrum, in which optical attenuation is small. These bands, windows, are in the region of big absorption. Early systems worked around 850 nm (first window). It was discovered that the second window (so called S band), 1310 nm, is more superior, because of smaller attenuation, and at the end the third window (C band) 1550 nm with smallest attenuation. Today the use of the fourth window (L band) 1625 nm is being discovered.

In the 80's started the idea of broadband WDM systems, that would use two broad-spaced wavelengths located around 1310 nm and 1550 nm (or 850 nm and 1310 nm). Narrowband WDM started in the 90's using two to eight channels. These channels are 400 GHz spaced in the 1550 nm window. Evolution continued during the 90's by developing dense WDM (DWDM) systems with 16 to 40 channels spaced 100 to 200 GHz. By the end of 90's these systems combined even 64 channels, dense packed with 50 GHz spacing. Crawford Hill laboratory was the first that reached the 1 TBps data speed in 1996, sending 50 channels, everyone with 20 GBps along the 55 km cable. [4]

### 3. STRUCTURE OF DWDM SYSTEMS

DWDM has few multilayer functions that are shown on the figure 1. It is a DWDM system with four channels. Every optical channel has its own wavelength.

Main functions of those systems are:

- **Generating the signal** – the source, semiconductor laser, assures that the light is in the specific narrow region that carries digital data, modulated as an analog signal.

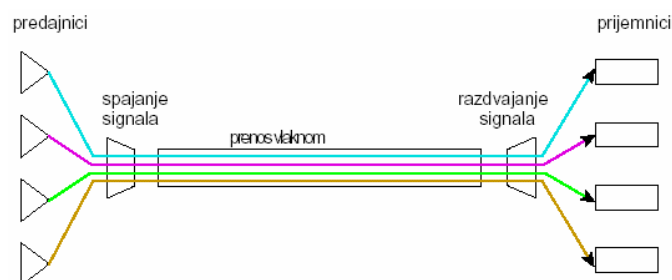


Figure 1. Functional scheme of DWDM

- **Signal combining** – modern DWDM systems use multiplexers to combine signals. One important thing is also the loss caused by multiplexing and demultiplexing, that depends of number of channels, but can be reduced by using optical amplifiers, that amplify all wavelengths at once without electro-optical conversion.
- **Transmitting the signal** – The effects of crosstalk, optical signal degradation and signal loss must be considered by planning the optic fiber transfer. These effects should be minimized by parameter controlling such as channel spacing, wavelength tolerance or laser power levels. Over a transmission link, the signal may need to be amplified.
- **Received signal separation** – On the receiver part, the multiplexed signals should be demultiplexed. Although it seems simpler than signal combining, process is technically more complicated.
- **Signal receiving** – The demultiplexed signal can now be received using photo detectors.

In addition to these functions, DWDM systems should also be equipped with transponders, which convert incoming signal in the form of monomode or multimode laser standard signal. [4]

### 4. TECHNIQUES

Technology development in the field of optical filters and narrowband lasers made it possible for DWDM systems to combine more than two wavelengths. By discovering optical amplifiers with flat gain, the transmitting distance had become bigger. Other technologies that had influence on the evolution of DWDM systems were optic fiber upgrading, with the result in smaller attenuation and better transmitting characteristics, also improvement of EDFA amplifiers and equipment like Bragg gratings used in the multiplexing process. [1]

#### Multiplexing and demultiplexing

The main idea of DWDM systems is that signals from different sources are transmitted through one fiber; multiplexer combines these incoming signals into one beam. Demultiplexer separates this beam to components with different wavelengths and routes them to fibers.

Demultiplexing has to be done before detecting the light, because photo detectors are broadband devices that cannot make selective detection of one specific wavelength.

**Techniques of multiplexing and demultiplexing**

A simple form of multiplexing or demultiplexing can be done using a **prism**. Figure 2 shows demultiplexing process. A parallel beam of polychromatic light is falling on a prism surface; each component wavelength is refracted differently. This is the "rainbow" effect. In the output light, each wavelength is separated from the next by an angle. A lens then focuses each wavelength to the point where it needs to enter a fiber. In the reverse process, the same components are used (multiplexing of different wavelengths onto one fiber).

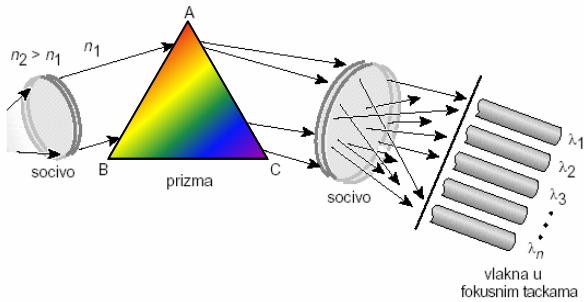


Figure 2. Demultiplexing, refracting through the prism

Another technology is based on the principles of **diffraction** and of **optical interference**. As shown on the figure 3 when polychromatic light enters a diffraction grating, each wavelength is diffracted at a different angle and therefore to a different point in place. Using a lens, these wavelengths can be focused onto individual fibers.

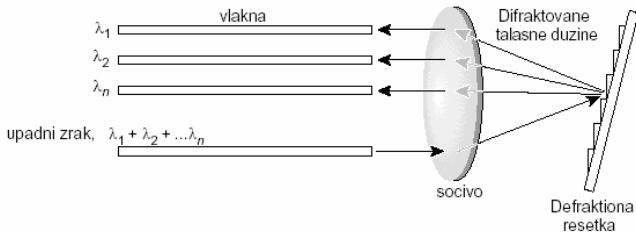


Figure 3. Grating Diffraction

**AWG** (arrayed waveguide gratings) device, also called an optical waveguide router consists of an array of curved-channel waveguides with a fixed difference in the path length between adjacent channels (shown at the figure 4).

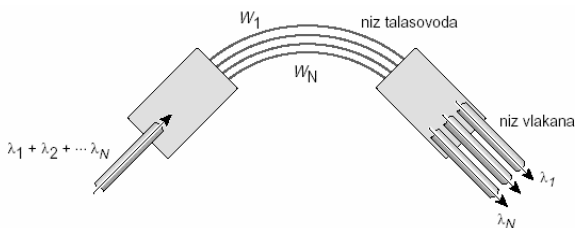


Figure 4. Arrayed Waveguide Grating (AWG)

Waveguides are connected to cavities at the input and output. When the light enters the input cavity, it diffracts and enters the waveguide array. There the optical length difference of each waveguide introduces phase delay in the output cavity, where an array of fibers is coupled. As results, different wavelengths are having maximal interference at different locations, which correspond to the output ports.

A different technology uses interference filters in devices called **thin film filters** or **multilayer interference filters**. By positioning filters, consisting of thin films, in the optical path, wavelengths can be sorted out (demultiplexed). The property of each filter is such that it transmits one wavelength while reflecting others. By cascading these devices, many wavelengths can be demultiplexed (see figure 5).

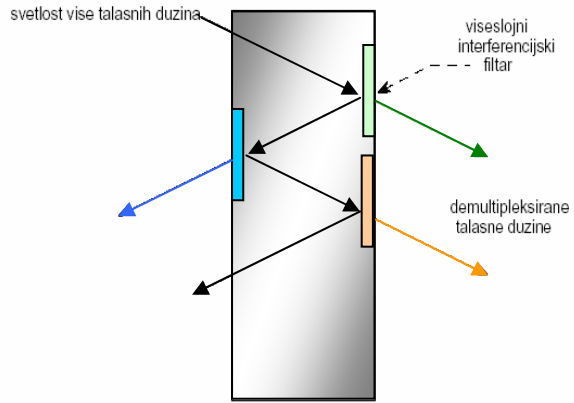


Figure 5. Multilayer interference filters

AWG and thin film interference filters are gaining prominence. Filters offer good stability and isolation between channels at moderate cost, but with a high insertion loss. AWGs are polarization-dependent (which can be compensated), and they exhibit a flat spectral response and low insertion loss. A potential drawback is that they are temperature sensitive such that they may not be practical in all environments. [4]

**Optical add/drop multiplexers**

In the DWDM systems, between multiplexing and demultiplexing, are different wavelengths being used. It is of interest that during transmitting some wavelengths could be dropped and other added. That is exactly what optical add/drop multiplexers (OADM) do.

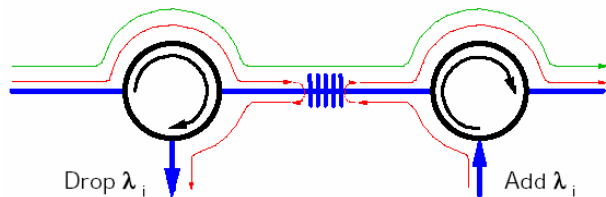


Figure 6. Selective dropping and adding of wavelength

Instead of separating and combining all wavelengths, OADM can drop some and other wavelengths are passed. OADMs are evolution key for all optical networks. OADM is similar to SONET and ADM, it adds and drops some wavelengths but it does not need any electro-optical conversion. Figure 6 shows that process. The signal should be amplified before and after the process, some OADM may have these amplifiers inside, depending on the manufacturer [2]

There are two types of OADM. First generation OADMs are fixed devices, which are physically configured to drop some specific wavelengths and to add other. The second generation of OADMs is variable and can dynamically choose which wavelengths to add and which to drop. Thin filter are chosen as filters for OADM in MAN DWDM systems because of their price and stability.

### Interleaving technology

Interleaving technology is used more and more, because it allows very dense channel packing with 50 GHz spacing or less. Two separate multiplexers or demultiplexers have channel spacing twice bigger than it is demanded at the output and they combine by interleaving, so that at the end the whole wavelength band is covered. One multiplexer (demultiplexer) covers even and other uneven channels (figure 7).

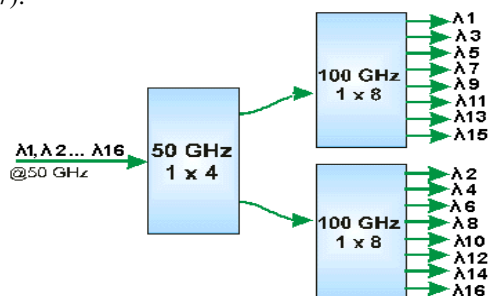


Figure 7. By the interleaving technique 50 GHz spacing is achieved using 100 GHz spacing demultiplexers

By using the interleaving technique, manufacturers can avoid making new components that request denser channel spacing and therefore they gain more profit.

General concept of interleaving is interferometer interleaving of two beams. Interference causes the periodically repeated signal on the output, if through the device wavelength multiples are passed and the wanted spacing is being achieved by additional model controlling.

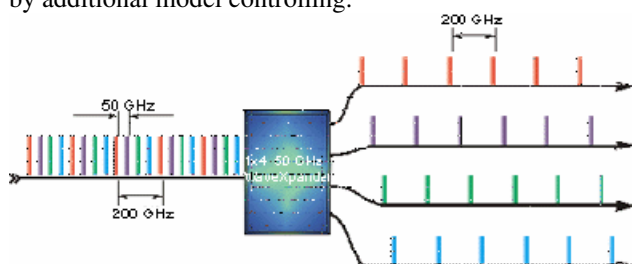


Figure 8. Interleaving 1x4

Logical upgrading of interleavers 1x2 would be interleavers 1x4. By this approach, it is possible to separate channels with 50 GHz spacing by using thin dielectric films or AWG filters with 200 GHz channel spacing (see figure 8).

Today, producers are using coupled fiber, liquid crystals and other materials. Possibly the easiest material and technology model are Mah-Zenderov interferometer coupled fibers. Interference appears between two fibers and is caused by their different length. By carefully controlling of distance between the lengths of fibers, wanted channel spacing will be accomplished according to the ITU table. These interleaves are made only of fibers, therefore they have very little attenuation, dispersion, uniform replay in spectrum of wavelength and they have minimal polarization effects [3].

Figure 9. shows the overview of multiplexing technology choice depending on different purpose. The choice of equipment and device for multiplexing and demultiplexing depends as on the number of channels as on the spacing between them, which are used in DWDM systems.

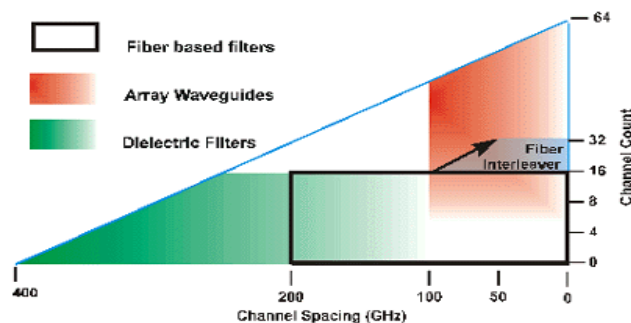


Figure 9. Choosing of DWDM technology depends of concrete usage

The criteria for choosing today's DWDM systems are often demanding usage of different techniques together, because of their own limitations.

## 5. COMPONENTS OF DWDM SYSTEMS

### Optical fibers

Optical monomode fibers eliminate dispersion between waves and it is possible to transfer signal on a big distance with less disfigures. Therefore, mostly monomode fibers are used in DWDM systems.

The main type of monomode optical fibers:

- **Non-dispersion-shifted fibers (NDSF)** – are used in more than 95% of networks; suitable are for TDM (one channel) in region of 1310nm or for DWDM in region of 1550nm (with the dispersion compensators)
- **Dispersions-shifted fibers (DSF)** – are suitable for TDM in region of 1550nm, however they are not suitable for DWDM in this window.
- **Non-zero dispersions-shifted fibers (NZ-DSF)** – are suitable also for TDM and DWDM in region of 1550nm.
- **Fibers of new generation** – these fibers allow the energy to go deeper in the cladding, allowing small dispersion in order to shrink mixing effects of four waves, these are also fibers with flat dispersion, which allows the usage of wavelength far from optimum wavelength, without spreading the impulse.

As the flow of data distribution has grown from 10GB/s to 40 GB/s, the number of so-called non linear effects is bigger, which shows that the signal changes on hard predictable way. [1]

### Sources and detectors of optical signals

There exist two light sources – LED diodes and lasers. Led diode is used only for small bit rates (less than 1GB/s) while the lasers might be used for much bigger bit rates.

Demands for lasers are: as precise wavelength, as narrow spectrum, big straight and control of chirp (change of signal frequency in time).

The type of modulation can influence the chirp. There are two semi conducting lasers, Fabry-Perot lasers and distributed feedback semiconductor lasers – DFB lasers. DFB lasers mostly are appropriate for DWDM systems because they are transmitting almost monochromatic light, they are capable to develop high bit rates, having good signal/noise rate and having good linearity. DFB lasers also have central frequency in the area of 1310nm and 1520-1565nm. The area from 1520

- 1565 nm is compatible with EDFA amplifier. DFB lasers are available for precise define wavelength.

At the receiver part it is necessary to detect the signal at each wavelength separately (signal is already de-multiplex). Photo detectors are big spectrum devices, example PIN or "lavin" photo diode.

**Optical amplifiers**

Because of the loss, the signals are transmitted on the limited distance.

**Erbium-doped fiber amplifiers (EDFA)**

Erbium-doped fiber amplifiers are necessary for successful transfer DWDM signals on big distance. Erbium is very rear element, which, when it is stimulated, emits the light on wavelength from 1.54µm and this is the wavelength on which the loss is lowest and which are used in DWDM. Attenuated signal enters erbium-doped fiber in which the light from 980nm or 1480nm is pumped in with the help of pump-laser. These stimulated atoms emit additional light at wavelength around 1550nm. As this process is continuing through the fiber, light becomes stronger. These stimulated emitted atoms of erbium make also the noise stronger. [1]

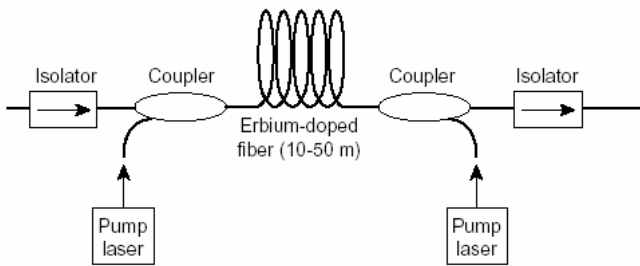


Figure 10. Erbium doped fiber amplifier

EDFA is available in C and L windows but in very small area (1530 – 1560nm). Because of it, the wavelengths are packed very tight, so that as much as possible channels can be transferred. Then mixing of channels becomes important and therefore it is necessary to make amplifier with bigger amplifier region so that channels can be more spaced.

That is exactly what EBFA (extended band fiber amplifier) stands for. It has one region same as by EDFA (1520 – 1560nm) and the other, extended at 1590nm. EBFA has flat gain in the region bigger then EDFA (35nm) and smaller noise. EBFA shows improvement, which is applicable in constant requests of bigger capacities.

**Ramanov amplifier**

Main ides is to use Ramanov effect. Raman effect happens by interaction of light and material (as e.g. fiber) and its effect is transferring some photons to others, usually bigger, wavelength.

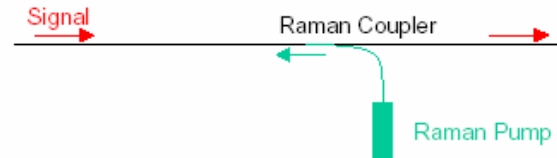


Figure 11. Raman amplifier

In this way, it is possible to amplify the signal by putting in light on a different smaller wavelength than the input signal has. Signal is being amplified when it passes the fiber with the same wavelength as the Raman emission (by input). Signals stimulate Ramanov emission, which is on the same wavelength as the signal, and so increase intensity of the signal. Raman amplifier has weak increase (big straight of laser for input is necessary), however it increases any wavelength (different then EDFA where it depends on erbium). By putting in more wavelengths, it is possible to reach very flat gain in big area.

**Linear optical amplifier**

New type of amplifier, LOA amplifier is first amplifier that is based on chip, and which has succeeded to handle the request on big number of DWDM channel without interfering. In addition, their attitude is predictable independently of changes in the net in real time and therefore they are acceptable for using in MAN and access networks.

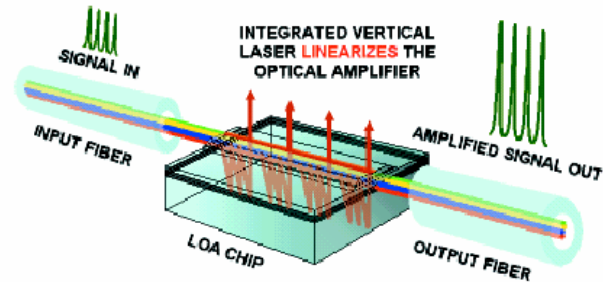


Figure 12. Linear optical amplifier

LOA is made from one optical active waveguide, which is connecting the entrance and outcome fibers. In the amplifier part, you can find also vertical laser, which is responsible for the linearity of this amplifier, and it behaves as ultra fast optical feedback that makes this amplifier flexible on changes in net. Light on more wavelengths is going vertical through chip; laser pump is going down vertically so that it increases all wavelengths. Future generations, which will be corrected outgoing force and decreased the noise, will be used in long-haul networks.

**Optical switches**

There are different technologies, which makes the optical switching possible. Some of them are already implemented in development phase. Here there will be detailed explained microelectronic method (MEMS switches) and the method based on technical crystal.

**MEMS optical switch**

There are technologies, which make optical switch possible. However, micro-electro-mechanic systems-based matrix optical switches – MEMS switches they are offering different advantages comparing to other.

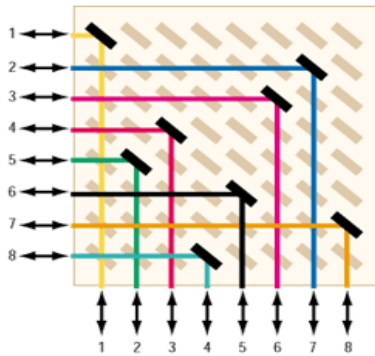


Figure 13. Matrix switch

First, it is based on silica and so is their production in big quantities and small dimensions (as semi conducting industry) cheap. In addition, MEMS switchers are working independently from wavelength and from protocol which is used. They are using simple optic in free space (moving mirrors and making it possible for any incoming channel to be transferred to any outgoing – figure 13.), so that the signals does not interfere with each other and the connection between them stays unaffected either referring to the transfer OC-192 (10GBps) signal or ATM signal. MEMS switchers are also bi-directional and so they can be used in different configurations. With the help of MEMS switchers dynamically add/drop multiplexes can be implemented.

### Other technology of optical switchers

Equipment that is based on liquid crystal solves the problem of electro-optical conversion. The main idea is in the polarization of the crystal: one type of polarization is being reflected while the other passes through. Then light travels through active region. If there is electromagnetic field active, it changes the polarization, if not, it does not change. Then these two streams (which polarization may have been changed) come to a combiner that passes light to specific outputs.

There are also commutators that are based on wavelength routers, lithium niobate or semi-conducting amplifiers. All of them have the same idea, that materials they are made of, change their optical characteristics (refraction index), if there is some electrical field present. Semi-conducting switchers are the fastest and therefore they are very suitable for WDM systems.

### 6. CONCLUSION

DWDM evolution is depending on compromises between characteristics, price and flexibility. There is no ideal technique but interleavers together with dielectrically filters or AWG are the future for DWDM systems. DWDM systems will guarantee the band for big data rates. Capacity will rise and allow bigger and bigger data rates and the only limit is the technology, like channel spacing.

DWDM is not only new technology now, it is the base for all optical networks that use network type of topology. This evolution is caused by commutation in photonic layer, and new routing protocols allow the light to travel through the network on the same way like in today's virtual networks. This all together give us a vision of all optical networks.

### 7. REFERENCE:

- [1] Kartalopoulos, Stamatios V. *Introduction to DWDM Technology: Data in a Rainbow*. New York: IEEE Press; 1999.
- [2] Agilent Technologies *Innovating the HP Way*, Dec 2000
- [3] Jerry Bautista and Robert Shine *Filter technologies via for DWDM system applications*, Wavesplitter Technologies Inc., June 2000
- [4] <http://www.iec.org/online/tutorials/dwdm/>
- [5] R.Ramaswami and Kumar N. Sivarajan *Routing and Wavelength Assignment in All-Optical Networks*, IEEE/ACM Transactions on Networking, Vol.3, no.5, October 1995

# INSTRUCTION FOR AUTHORS

*Name of the author/s, Affiliation/s*

**Abstract:** *Short instruction for authors is presented in this paper. Works that are to be printed in the review "Electronics" should be typed according to this instruction.*

**Keywords:** *Review Electronics, Faculty of Electrical Engineering in Banjaluka, Instruction for authors.*

## 1. INTRODUCTION

In the review "Electronics", we publish the scientific and professional works from different fields of electronics in the broadest sense like: automatics, telecommunications, computer techniques, power engineering, nuclear and medical electronics, analysis and synthesis of electronic circuits and systems, new technologies and materials in electronics etc. In addition to the scientific and professional works, we present new products, new books, B. Sc., M. Sc. and Ph.D. theses.

In order to enable the unification of the technical arrangement of the works, to simplify the printing of the review "ELECTRONICS", we are giving this instruction for the authors of the works to be published in this professional paper.

## 2. TECHNICAL DETAILS

### 2.1. Submitting the papers

The works are to be delivered to the editor of the review by the E-mail (elektronika@etfbl.net) or on floppy (or CD) by post mail to the address of the Faculty of Electrical Engineering (Elektrotehnicki fakultet, Patre 5, 78000 Banja Luka, Republic of Srpska, Bosnia and Herzegovina).

### 2.2. Typing details

The work has to be typed on the paper A4 format, 8.27" width and 11.69" height (21.0x29.7 cm), upper margin of 1" (2.54 cm) and lower margin of 0.59" (1.5 cm), left and right margins of 1.57" (2 cm) and 0.39" (1cm) (mirrored margins). The header and footer are 0.5" (1.27cm) and 57" (2 cm). The work has to be written in English language. Our suggestion to the authors is to make their works on a PC using the word processor MS WORD 97/2000, and for the figures to use the graphic program CorelDraw, if the graphs are not going from the original programs, i.e., from the programs received (like MATLAB).

The title of the work shall be written on the first page, in bold and 12 pt. size. Also, on the first page, moved for one line spacing from title, the author's name together with the name of his institution shall be printed in the letter size (10pt, *Italic*). The remaining parts of the manuscript shall be done in two columns with 0.5cm distance. The work shall be typed with line spacing 1 (Single) and size not less than 10 pt (like as this instruction). After the title of the work and the name of the author/s, a short content in English language follows, written in italics. The subtitles in the text shall be written in bold, capital letters of the size as in the text (not less than 10 pt.). Each work shall, at the beginning, comprise a subtitle INTRODUCTION, and, at the end, the subtitles CONCLUSION and BIBLIOGRAPHY / REFERENCES.

The operators and size marks that do not use numerical values, shall be written in common letters. The size marks that can use numerical values shall be written in italics. The equations shall be written in one column with right edge numeration. If the breaking of equations or figures is desired, those may be placed over both columns.

Illustrations (tables, figures, graphs etc.) may be wider than one column if necessary. Above a table there shall be a title, for instance: Table 2. *The experimental measuring results*. The same applies to figures and graphs but the accompanying text comes underneath the figure of graphs, for instance: Fig.3: *Equivalent circuit diagram...*

The work should not be finished at the beginning of a page. If the last manuscript page is not full, the columns on that page should be made even. Number of pages should not go over 6.

## 3. CONCLUSION

This short instruction is presented in order to enable the unification of technical arrangement of the works.

## 4. REFERENCES

At the end of work, the used literature shall be listed in order as used in the text. The literature in the text, shall be enclosed in square brackets, for instance: ...in [2] is shown ...

# ELECTRONICS

Vol. 7, No. 1, September 2003.

## CONTENTS

<b>PREFACE .....</b>	<b>1</b>
<b>BIOGRAPHY OF GUEST EDITOR .....</b>	<b>2</b>

*Selected papers from the Symposium INFOTEH® – JAHORINA 2003*

<b>OPTICAL FLIP-FLOP OSCILLATOR WITH COMPLEX COUPLING CONSTANT.....</b>	<b>3</b>
<b>Zoran Ljuboje, Milan Petrović</b>	
<b>STRUCTURAL MODELING OF HYDRAULIC SYSTEMS.....</b>	<b>6</b>
<b>Dragan H. Pršić, Novak N. Nedić</b>	
<b>AN ALGORITHM FOR OFF-NOMINAL FREQUENCY MEASUREMENTS IN ELECTRIC POWER SYSTEMS.....</b>	<b>11</b>
<b>Milenko B. Đurić, Željko R. Đurišić</b>	
<b>WORKSPACE FOR FUTURE E-SCIENTISTS: GRID AND MYGRID .....</b>	<b>15</b>
<b>Milena Radenković</b>	
<b>SPECIAL NOISE REDUCTION DIGITAL FILTERS IMPLEMENTATION .....</b>	<b>18</b>
<b>Darko Nikolić, Petar Rajković, Dragan Janković</b>	
<b>SOME POSSIBILITIES OF ARBITRARY WAVEFORM SYNTHESIS FOR DPS SYSTEMS .....</b>	<b>23</b>
<b>Bosiljka Vukčević</b>	
<b>EXTENSION OF THE INPUT VOLTAGE RANGE OF FLYBACK CONVERTER BY MEANS OF IGBT .....</b>	<b>25</b>
<b>Vladimir Rajović, Nenad Jovičić, Slavoljub Marjanović</b>	
<b>COMPARATIVE CHARACTERISTICS OF THICK FILM LC FILTERS WITH DIELECTRIC AND FERRITE LAYER.....</b>	<b>27</b>
<b>Vladan Desnica, Ljiljana Živanov, Obrad Aleksic, Miloljub Luković, Lazar Lukić</b>	
<b>IMPROVED METHOD FOR OPTIMISATION OF INDUCTORS USING GEOMETRIC PROGRAMMING .....</b>	<b>31</b>
<b>Goran Stojanovic, Ljiljana Živanov, Mirjana Damnjanovic</b>	
<b>STRUCTURE, TECHNOLOGIES AND COMPONENTS OF DWDM SYSTEMS.....</b>	<b>35</b>
<b>Ivanković Snežana</b>	